

Dynamical classification of topological quantum phases

Lin Zhang,^{1,2,*} Long Zhang,^{1,2,*} Sen Niu,^{1,2} and Xiong-Jun Liu^{†1,2}

¹*International Center for Quantum Materials, School of Physics, Peking University, Beijing 100871, China.*

²*Collaborative Innovation Center of Quantum Matter, Beijing 100871, China.*

Topological phase of matter is now a mainstream of research in condensed matter physics, of which the classification, synthesis, and detection of topological states have brought many excitements over the recent decade while remain incomplete with ongoing challenges in both theory and experiment. Here we propose to establish a universal dynamical characterization of the topological quantum phases classified by integers, with the framework of the study consisting of basic theorems. First, we uncover that classifying a generic d -dimensional (dD) gapped topological phase can reduce to a $(d-1)D$ invariant defined on so-called band inversion surfaces (BISs), rendering a fundamental *bulk-surface* duality. Further, we show in quenching across phase boundary the (pseudo)spin dynamics to exhibit unique topological patterns on BISs, which are attributed to the post-quench bulk topology and manifest a dynamical *bulk-surface* correspondence. The topological phase is then classified by a dynamical topological invariant measured from dynamical spin-texture field on the BISs. Applications to quenching experiments on feasible models are proposed and studied. This work opens a new direction to classify and detect topological phases by quantum dynamics.

In the last over thirty years, following the discovery of the quantum Hall effect [1, 2], physicists have established a new classification of fundamental states of quantum matter, called topological quantum phases [3, 4], which are beyond the scope of the celebrated Landau-Ginzburg-Wilson framework that characterizes quantum matter by local symmetry-breaking orders [5]. A topological quantum phase can be classified by bulk topological invariant defined for its ground state at equilibrium, and hosts protected boundary modes through the bulk-boundary correspondence [6, 7]. This characterization crucially influences the strategies of identifying topological states in experiment, which is challenging in general since the non-local topological invariants may not have direct physical measurements. Despite the great success achieved with various strategies in discovering new topological matter, such as topological insulators [8–11] and semimetals [12, 13] whose boundary modes can be probed by transport measurement or angle resolved photoemission spectroscopy, by far only a small portion of topological states predicted in theory have been uncovered in experiment [14]. In some circumstances the measurements are not fully unambiguous for being not direct observations of topological numbers, for which there are topological states, e.g., the topological superconductors [15–19], even well explored in theory, necessitating further experimental confirmation.

As yet, the topological states have been primarily characterized based on classification theories developed for equilibrium systems, ranging from symmetry-protected topological phases [20, 21] to intrinsic topological orders [4]. A fundamental question arises that, for a generic topological quantum phase defined in equilib-

rium, is there a non-equilibrium classification of such state? We address this fundamental issue in the present work, and establish a dynamical classification theory for topological quantum phases characterized by integers of all dimensions. Besides the explicit fundamental significance, the dynamical classification is also experimentally important in probing new topological quantum physics, particularly relevant for ultracold atom systems where, due to heating, the equilibrium ground states are usually hard to achieve, but the quantum dynamics can be readily engineered. In particular, the recent experiments demonstrated the feasibility of simulating novel topological systems with quantum gases, including the 1D Su-Schrieffer-Heeger (SSH) chain [22, 23], 1D chiral topological phase [24, 25], and 2D Chern insulators [26–29], and observing topology via quantum dynamics although valid in very special cases [25, 30, 31].

The framework of the dynamical classification theory is made up of several fundamental theorems uncovered in this work. First, for a generic d -dimensional (dD) gapped topological phase characterized by integer invariants, we show a *bulk-surface* duality that its classification reduces to a $(d-1)D$ invariant defined on so-called band inversion surfaces (BISs). Further, in quenching from trivial to topological phases, the BISs are captured by a dynamical characterization that the time-averaged spin-polarizations vanish on BISs in the unitary evolution. Finally, the bulk topology of the post-quench phase is classified by the dynamical topological invariant determined via an emergent dynamical (pseudo)spin-texture field on BISs. The results manifest a dynamical *bulk-surface* correspondence which can be directly measured with high feasibility in quenching experiments.

Generic model.—We start with the generic d -dimensional (dD) gapped topological phases, including insulators and superconductors, which are classified by integer invariants in the Altland-Zirnbauer (AZ) symme-

[†]Corresponding author: xiongjunliu@pku.edu.cn

try classes [32–35]. The basic Hamiltonian can be written in the elementary representation matrices of the Clifford algebra [36, 37]

$$\mathcal{H}(\mathbf{k}) = \vec{h}(\mathbf{k}) \cdot \vec{\gamma} = \sum_{i=0}^d h_i(\mathbf{k}) \gamma_i, \quad (1)$$

where the $\vec{\gamma}$ matrices define a (pseudo)spin obeying anti-commutation relation $\{\gamma_i, \gamma_j\} = 2\delta_{ij}\mathbb{1}$, with $i, j = 0, 1, \dots, d$, and $\vec{h}(\mathbf{k})$ mimics a $(d+1)$ D Zeeman field depending on the Bloch momentum \mathbf{k} in BZ. The dimensionality of γ matrices in the elementary representation reads $n_d = 2^{d/2}$ (or $2^{(d+1)/2}$) if d is even (or odd), which is the minimal requirement to open a topological gap for the d D topological phase [37]. In the 1D and 2D regimes, for instance, the γ matrices simply reduce to the Pauli ones, and $\mathcal{H}(\mathbf{k})$ describes a two-band model for the topological states, e.g., the well-known SSH model [22, 35] for 1D BDI class insulator and the Haldane model [38] for 2D Chern insulator. Similarly, for 3D and 4D phases, the γ matrices take the Dirac forms, and a fully gapped topological phase has to involve at least four bands, such as the 3D AIII class topological insulator (also DIII class superconductors) [33, 39] and 4D quantum Hall effect [40]. While for convenience our theory is formulated with the basic Hamiltonian written in the above elementary representation, we can show that in classifying the topology, any generic multiband model of the d D phase can be decomposed into direct sum of the above basic Hamiltonian. Therefore, all the main results presented based on Eq. (1) directly apply to the generic d D gapped topological phases characterized by integer invariants (see details in Supplementary Material [41]).

To facilitate the discussion and without loss of generality, we pick up one component, say $h_0(\mathbf{k})$, from the vector field $\vec{h}(\mathbf{k})$ to characterize the ‘dispersion’ of the n_d decoupled bands. Accordingly, we denote the remaining components of $\vec{h}(\mathbf{k})$ as the ‘spin-orbit’ (SO) field $\mathbf{h}_{\text{so}}(\mathbf{k}) = (h_1, \dots, h_d)$. Without the SO field, the band crossing occurs for the n_d decoupled bands if $h_0(\mathbf{k}) = 0$ results at certain momentum points of the BZ. All such momentum points form closed $(d-1)$ D surface, dubbed *band inversion surface* (BIS), which is a key notation in this work. In the generic case one can have multiple BISs in the first BZ. Across the BIS the energy difference between half of the n_d bands and the remaining half switches sign. The gap opens when the nonzero SO field $\mathbf{h}_{\text{so}}(\mathbf{k})$ is switched on in the BISs. As shown below, the d D gapped phase being topologically nontrivial necessitates that the BZ includes at least one BIS which hosts a nonzero $(d-1)$ D invariant.

Topological characterization on BISs.—The topology of the Hamiltonian $\mathcal{H}(\mathbf{k})$ is classified by d D winding number for odd dimensionality $d = 2n - 1$, or the n -th Chern number if the dimension is even with $d = 2n$ [41]. The topological characterization of the equilibrium phase

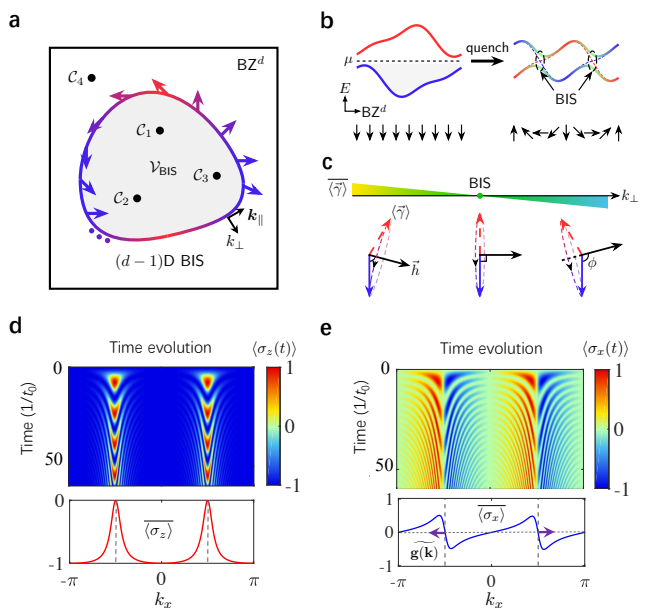


Figure 1: Dynamical bulk-surface correspondence and the 1D exemplification. **a**, The d -dimensional topological phases classified by \mathbb{Z} can be characterized by the winding of the SO field (colored arrows) on the $(d-1)$ -dimensional BISs, which counts the total topological charges C_i of the SO field in the region \mathcal{V}_{BIS} (gray) enclosed by BISs with $h_0 < 0$. Here the momentum \mathbf{k} is decomposed into $(k_{\perp}, k_{\parallel})$ (black arrows) with k_{\perp} perpendicular to the BIS and pointing to the complementary region of \mathcal{V}_{BIS} , i.e., $\bar{\mathcal{V}}_{\text{BIS}}$ with $h_0 > 0$. **b-c**, Detecting topological patterns on the BISs by quench dynamics. A quench process is employed, where a trivial system with highly polarized (pseudo)spins in the negative direction of the axes h_0 is suddenly quenched to a topological band with nontrivial spin textures **(b)**. Subsequently, dramatic spin precession occurs near the BISs with the rotation axis being the post-quench vector field $\vec{h}(\mathbf{k})$ **(c)**. The SO field is encoded by the variation of time-averaged spin polarizations $\langle \vec{\gamma} \rangle$ with respect to k_{\perp} . Here the blue and red dashed lines in **b** represent the h_0 component of the post-quench Hamiltonian with the band crossing being the $(d-1)$ D BIS, and ϕ in **c** denotes the relative angle between the initial spin (blue) and the post-quench vector field $\vec{h}(\mathbf{k})$. **d-e**, Numerical results for the 1D model. Time evolution (upper panel) and the corresponding averages (lower panel) of spin textures are shown after a sudden quench from $m_z = 8t_0$ (trivial) to 0 (topological) with $t_{\text{so}} = 0.2t_0$. The BIS is determined by momenta with vanishing time-averaged spin polarizations $\langle \overline{\sigma_{x,z}} \rangle$ (dashed lines), and the new dynamical spin-texture field $\mathbf{g}(\mathbf{k}) = -\partial_{k_{\perp}} \langle \overline{\sigma_x} \rangle$ (purple arrows in **e**) characterizes the nontrivial topology.

is formulated by a mapping from the BZ, which is a d D torus T^d , to the d D spherical surface S^d through the unit vector field $\mathbf{n}(\mathbf{k}) = \vec{h}/|\vec{h}|$. The topological number counts the times that the mapping covers the spherical surface S^d . Remarkably, as detailed in the Supplementary Material [41], we show that the topological characterization (by d D winding number or Chern number) generically

reduces to a $(d-1)$ D invariant w_{d-1} on the BISs

$$w_{d-1} = \sum_j \frac{\Gamma(d/2)}{2\pi^{d/2}} \frac{1}{(d-1)!} \int_{\text{BIS}_j} \hat{\mathbf{h}}_{\text{so}}(d\hat{\mathbf{h}}_{\text{so}})^{d-1}, \quad (2)$$

where $\Gamma(x)$ is the Gamma function, $\hat{\mathbf{h}}_{\text{so}}(\mathbf{k}) = \mathbf{h}_{\text{so}}/|\mathbf{h}_{\text{so}}|$ is the normalized SO field, and ‘d’ in the integrand denotes the exterior derivative. The integral performed on the j -th closed BIS yields the integer times that $\hat{\mathbf{h}}_{\text{so}}$ -field covers over the $(d-1)$ D spherical surface S^{d-1} when \mathbf{k} runs over the j -th BIS. Without giving details, we show the above invariant w_{d-1} intuitively by clarifying the key ingredients of the theorem, while the rigorous proof can be found in the Supplementary Material [41]. As for topological phase, the mapping $T^d \mapsto S^d$ covers nonzero integer times of the d D spherical surface, any component of the vector field $\vec{h}(\mathbf{k})$, including $h_0(\mathbf{k})$, spans both positive and negative values in the BZ. Thus the BIS with $h_0(\mathbf{k}) = 0$ must be obtained. It is convenient to denote by \mathcal{V}_{BIS} the vector volume of the BZ with $h_0(\mathbf{k}) < 0$, and $\bar{\mathcal{V}}_{\text{BIS}}$ the volume with $h_0(\mathbf{k}) > 0$. The right hand side of Eq. (2) represents a $(d-1)$ D surface integral enclosing the vector volume \mathcal{V}_{BIS} , and the invariant w_{d-1} counts the total topological charges located at the singularities with $\mathbf{h}_{\text{so}}(\mathbf{k}) = 0$ in this volume [see Fig. 1a]. This result can be intuitively understood in the following way, for which we rewrite that $h_0(\mathbf{k}) = m_0 + \tilde{h}_0(\mathbf{k})$, with \tilde{h}_0 being momentum-dependent and m_0 mimicking a constant ‘magnetization’ which tunes the topology of the phase. It is readily to know that when $m_0 > \max[|\tilde{h}_0(\mathbf{k})|]$ for all \mathbf{k} , the phase is trivial since no BIS can be obtained in the BZ. The BIS starts to emerge in the BZ by reducing the magnetization to $m_0 \lesssim \max[|\tilde{h}_0(\mathbf{k})|]$, while the gap of the system keeps open if no topological charges (at $\mathbf{h}_{\text{so}}(\mathbf{k}) = 0$) enter the vector volume \mathcal{V}_{BIS} . Further reducing m_0 eventually enables that the topological charges pass through the BIS and enter the volume $\bar{\mathcal{V}}_{\text{BIS}}$. Note that when a topological charge crosses the BIS, the bulk gap closes one time since $h_0 = \mathbf{h}_{\text{so}} = 0$ occurs at the crossing momentum on the BIS. This leads to a topological phase transition with the topological invariant varying by one. Then the number of topological charges with $\mathbf{h}_{\text{so}}(\mathbf{k}) = 0$ enclosed in the volume \mathcal{V}_{BIS} reflects the times of gap closing by tuning m_0 from trivial to the final topological regime, and the total topological charge gives the bulk topological number of the phase, as characterized by the theorem formulated in Eq. (2).

The above theorem shows a fundamental *bulk-surface* duality which maps the classification of bulk topology to the characterization on BISs. The bulk-surface duality provides a much simplified characterization of the topological phases with lower-dimensional invariants. Nevertheless, there are important issues which should be addressed. While the BISs are well defined, how to precisely identify them in a real experiment, which is clearly necessary to further measure topological numbers, is by no

means trivial. As we show below that, the uncovered bulk-surface duality is further mapped to the dynamical form in the non-equilibrium quench dynamics, which provide direct measurement of all the topological features.

Non-equilibrium classification: dynamical bulk-surface correspondence.—We proceed to consider the non-equilibrium characterization of topological phases based on the bulk-surface duality shown above. The quantum dynamics can be induced by quenching the phase from a deep initially trivial phase at time $t = 0$, which is given by setting $m_0|_{t<0} \gg \max[|\vec{h}(\mathbf{k})|]$, to the final topological state which is obtained in proper regime $|m_0|_{t>0} < \max[|h_0(\mathbf{k})|]$ [Fig. 1(b)]. The unitary evolution of the (pseudo)spin $\vec{\gamma}$ is then governed by the post-quench Hamiltonian $\mathcal{H}(m_0, \mathbf{k})$. The quenching dynamics can be quantified by introducing the dynamical averaging of the spin-polarization, which is obtained by

$$\overline{\langle \gamma_i(\mathbf{k}) \rangle} = \lim_{T \rightarrow \infty} \frac{1}{T} \int_0^T dt \text{Tr} [\rho_0 e^{i\mathcal{H}t} \gamma_i e^{-i\mathcal{H}t}], \quad (3)$$

where ρ_0 is density of matrix of the initial state. The peculiar effects are obtained on the BISs. Note that the system is initialized in the fully spin-polarized phase with the (pseudo)spin of all Bloch states pointing along negative h_0 axis (for positive m_0). The spin precesses with respect to $\vec{h}(\mathbf{k})$ after quenching. On the BISs, the vector $\vec{h}(\mathbf{k}) = \mathbf{h}_{\text{so}}(\mathbf{k})$ is perpendicular to initial spin polarization, which leads to the precession of the spin vector $\vec{\gamma}$ within the plane perpendicular to \mathbf{h}_{so} while incorporating $h_0(\mathbf{k})$ axis [Fig. 1(c)]. As a result, the dynamical averaging $\overline{\langle \gamma_i \rangle}$ vanishes right on the BISs for all i -components. On the other hand, at the momentum \mathbf{k} away from the BISs the h_0 component is nonzero, so \vec{h} is not perpendicular to the initial spin polarization. Then the spin precession leads to a nonzero $\overline{\langle \vec{\gamma} \rangle}$ along the $\vec{h}(\mathbf{k})$ -direction [Fig. 1(c)]. With these results we conclude a dynamical characterization of the BISs that

$$\overline{\langle \gamma_i(\mathbf{k}) \rangle} = 0, \quad \text{for } \mathbf{k} \in \text{BISs}, \quad i = 0, 1, 2, \dots, d. \quad (4)$$

The above characterization can also be understood that on BISs, the resonant spin-reversing transitions $\vec{\gamma} \rightarrow -\vec{\gamma}$ are induced by the SO field $\mathbf{h}_{\text{so}}(\mathbf{k})$ due the vanishing gap (for band-crossing surfaces). Thus the time-averaged spin-polarizations vanish at BISs. In contrast, away from the BISs, the nonzero $h_0(\mathbf{k})$ severs as a detuning for the spin-reversing transitions, so the time-averaged spin-polarizations do not vanish.

The vanishing $\overline{\langle \gamma_i \rangle}$ on BIS implies that the topological number of the d D gapped phase cannot be obtained via the time-averaged spin-texture $\overline{\langle \vec{\gamma}(\mathbf{k}) \rangle}$. Interestingly, more nontrivial features of the quench dynamics are captured by the *variation* of the time-averaged spin polarizations across the BISs. Note that the component $h_0 < 0$ in the vector volume \mathcal{V}_{BIS} and $h_0 > 0$ in the volume $\bar{\mathcal{V}}_{\text{BIS}}$. When passing through a BIS, the relative angle ϕ

between the initial spin-polarization and the vector $\vec{h}(\mathbf{k})$ varies from $\phi < \pi/2$ in \mathcal{V}_{BIS} , with a nonzero dynamical averaging $\langle \vec{\gamma} \rangle$ pointing to $\vec{h}(\mathbf{k})$ -direction, to $\phi > \pi/2$ in $\bar{\mathcal{V}}_{\text{BIS}}$, with nonzero $\langle \vec{\gamma} \rangle$ pointing oppositely to $\vec{h}(\mathbf{k})$ -direction [Fig. 1(c)]. This follows that the variation of $\langle \vec{\gamma} \rangle$ across the BIS follows the direction of the spin-orbit field \mathbf{h}_{SO} . To quantify this picture, we define a new dynamical spin-texture field $\widetilde{\mathbf{g}}(\mathbf{k})$, whose components are given by $g_i(\mathbf{k}) \equiv -\frac{1}{\mathcal{N}_{\mathbf{k}}} \partial_{k_{\perp}} \langle \gamma_i \rangle$, with $\mathcal{N}_{\mathbf{k}}$ being the normalization factor. Here k_{\perp} denotes the momentum perpendicular to BIS and points from \mathcal{V}_{BIS} to $\bar{\mathcal{V}}_{\text{BIS}}$. It can be shown from Eq. (3) that on the BISs [41]

$$\widetilde{g}_i(\mathbf{k})|_{\mathbf{k} \in \text{BISs}} = \hat{h}_{\text{so},i}(\mathbf{k}). \quad (5)$$

With this identity we reach immediately that the topological invariant defined on the BISs can be recast into a dynamical form, namely

$$w_{d-1} = \sum_j \frac{\Gamma(d/2)}{2\pi^{d/2}} \frac{1}{(d-1)!} \int_{\text{BIS}_j} \widetilde{\mathbf{g}}(\mathbf{k}) [d\widetilde{\mathbf{g}}(\mathbf{k})]^{d-1}. \quad (6)$$

The right hand side of the above formula describes the mapping from BISs to $(d-1)$ D spherical surface which the emergent dynamical field $\widetilde{\mathbf{g}}(\mathbf{k})$ belongs to, rendering the dynamical classification of the d D gapped phase. The dynamical topological invariant is intuitively described by the coverage of the emergent spin-texture $\widetilde{\mathbf{g}}(\mathbf{k})$ over the full $(d-1)$ D spherical surface [41]. The results in Eqs. (4)-(6) manifest a novel dynamical *bulk-surface* correspondence, which can be directly measured from the dynamical spin-polarization patterns emerging on the BISs. In the following, we demonstrate measuring the bulk topology by the dynamical classification with experimentally feasible models.

Application to quenching experiments.—We first consider the 1D topological phases of AIII class obtained by the Hamiltonian $\mathcal{H}(k_x) = \vec{h}(k_x) \cdot \vec{\sigma}$, where $h_x = t_{\text{SO}} \sin k_x \equiv h_{\text{SO}}$, $h_y = 0$, and $h_z = m_z - t_0 \cos k_x \equiv h_0$, with t_0 and t_{SO} denoting the nearest-neighbor spin-conserved and spin-flipped hopping coefficients. The model was proposed in Ref. [24] and realized recently in experiment for ^{173}Yb fermions [25]. The effective magnetization m_z can be precisely tuned by a bias magnetic field. The quench study is performed by tuning the Zeeman term from $m_z \gg t_0$, which corresponds to the deep trivial regime with the system initialized in spin-down, to $|m_z| < t_0$, which lies in topological regime. The quantum dynamics is then governed by the unitary evolution operator (see Methods). The numerical results are shown in Fig. 1d-e, with the parameters taken as $t_{\text{SO}} = 0.2t_0$. The resonant spin-flip transitions driven by SO field emerge at two momentum points $k_{\text{BIS}} = \pm \cos^{-1}(m_z/t_0)$ with vanishing time-averaged spin polarizations $\langle \vec{\sigma} \rangle$, which manifests the BIS (band inversion points). Away from the BIS the spin-flip oscillation is well suppressed by the energy

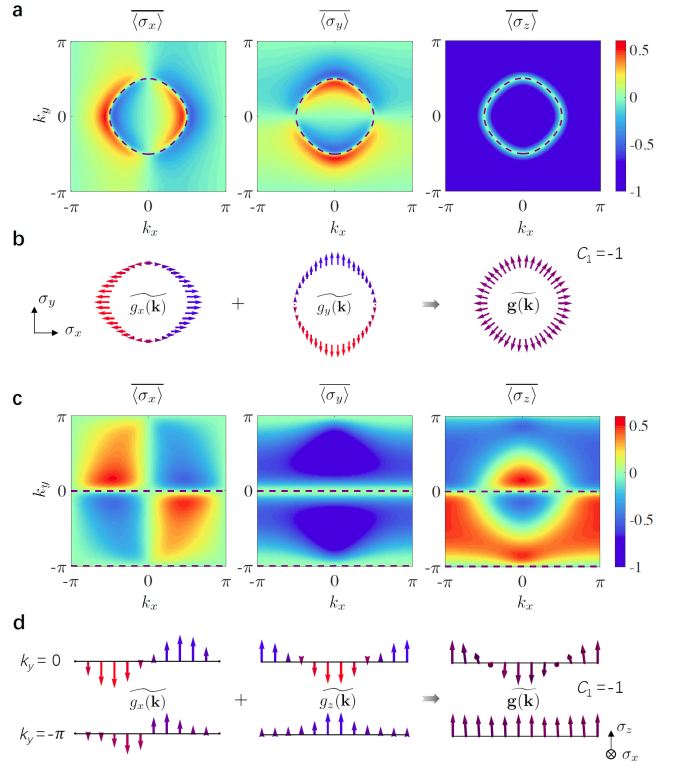


Figure 2: Characterizing 2D Chern insulators in different quench processes. **a-b**, Topological patterns by quenching along $h_z(\mathbf{k})$ axis. Time-averaged spin textures **(a)** are measured after a sudden quench from $m_z = 8t_0$ to t_0 ($m_x = m_y = 0$, $t_{\text{SO}}^{x,y} = 0.2t_0$), with BIS being characterized by $\langle \vec{\sigma} \rangle = 0$ (green ring). The dynamical field $\widetilde{\mathbf{g}}(\mathbf{k})$ obtained from **a** indicates the Chern number $C_1 = -1$ **(b)**. **c-d**, Topological patterns by quenching $h_y(\mathbf{k})$ axis. Time-averaged spin textures **(c)** and the dynamical field on the BIS **(d)** are shown after a quench from $m_y = 50t_0$ to 0, with $m_z = t_0$, $m_x = 0$, and $t_{\text{SO}}^x = 0.5t_{\text{SO}}^y = t_0$. Here the two BISs are at $k_y = 0, -\pi$. While the winding of $\widetilde{\mathbf{g}}(\mathbf{k})$ is trivial along $k_y = -\pi$, the non-zero winding number along $k_y = 0$ characterizes the topological phase with the Chern number $C_1 = -1$.

gap. The opposite magnitudes of the directional derivative $\partial_{k_{\perp}} \langle \sigma_x \rangle$ at two band inversion points show the non-trivial topology of the post-quench regime, and gives the winding number $+1$ for $|m_z| < t_0$ (Fig. 1 e) [41].

In two dimensions, we consider the quantum anomalous Hall model [42] realized in recent experiments [28, 29] $\mathcal{H}(\mathbf{k}) = \vec{h}(\mathbf{k}) \cdot \vec{\sigma}$, where the vector field reads $\vec{h}(\mathbf{k}) = (m_x + t_{\text{SO}}^x \sin k_x, m_y + t_{\text{SO}}^y \sin k_y, m_z - t_0 \cos k_x - t_0 \cos k_y)$. The flexibility in the decomposition of the vector $\vec{h}(\mathbf{k})$ allows us to consider different quench ways, e.g., by quenching h_z or h_y axis. First, we take $h_0 \equiv h_z$, $\mathbf{h}_{\text{SO}} \equiv (h_x, h_y)$, and the quench is performed by varying magnetization suddenly from $m_z \gg t_0$ to $0 < |m_z| < 2t_0$, while setting $m_x = m_y = 0$. Similar to 1D model, the resonant transition between the spin-down and spin-up states only occurs at the BIS (band inversion ring). From

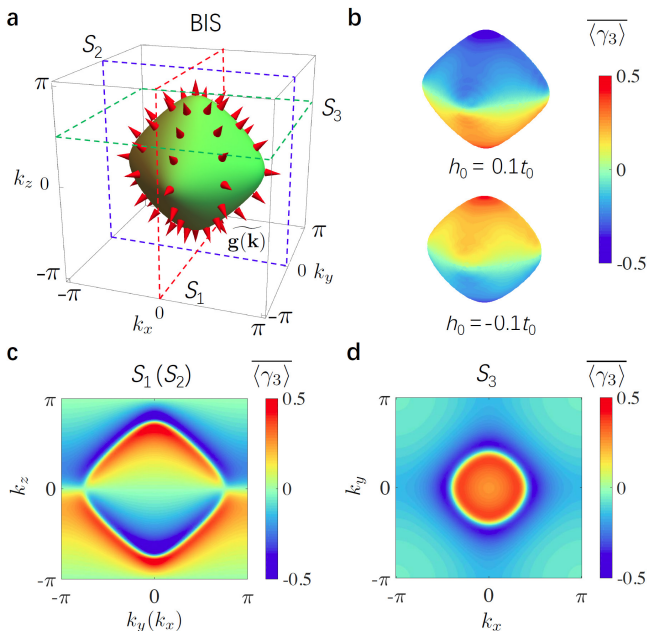


Figure 3: 3D chiral topological phases. **a**, The BIS (green sphere) defined by $h_0(\mathbf{k}) = 0$ and the emergent dynamical (pseudo)spin-texture field $\mathbf{g}(\mathbf{k})$ (red arrows) are shown for $m_z = 1.3t_0$ and $t_{\text{so}} = 0.2t_0$. **b**, The $\mathbf{g}(\mathbf{k})$ field is dynamically measured from variation of spin textures at two equal-energy surfaces at $h_0 = \pm 0.1t_0$, with the time-averaged spin textures $\langle \gamma_3 \rangle$ being given. **c-d**, Time-averaged spin textures $\langle \gamma_3 \rangle$ in cross sections $k_{x,y} = 0$ ($S_{1,2}$ in **c**) and $k_z = \frac{\pi}{2}$ (S_3 in **d**). Here the quench is taken from $m_z = 8t_0$ to $1.3t_0$ and spin textures $\langle \gamma_{1,2} \rangle$ are shown in Supplementary Materials.

the numerical results given in Fig. 2 a, with $m_z = t_0$ and $t_{\text{so}}^{x,y} = 0.2t_0$, the vanishing time-averaged spin-polarizations $\langle \sigma_i \rangle = 0$ are clearly shown in the BIS. Furthermore, the emergent dynamical field $\mathbf{g}(\mathbf{k}) = -\partial_{k_\perp} \langle \vec{\sigma} \rangle$ exhibits a nonzero 1D winding on the BIS, which characterizes a topological charge located at Γ point [with $\mathbf{k} = (0,0)$] and gives the Chern number $C_1 = -1$ (Fig. 2 b). On the other hand, if $-2t_0 < m_0 < 0$ for the post-quench regime, an opposite dynamical winding exhibits on the BIS which circles M point [with $\mathbf{k} = (\pi, \pi)$], and gives $C_1 = +1$ (see Supplementary Material [41]). Secondly, we take $h_0 \equiv h_y$ and quench the h_y axis by ramping m_y quickly from $m_y \gg t_0$ to $m_y = 0$, while setting $m_x = 0$ and $m_z = t_0$. The time-averaged dynamical spin textures exhibit line-shape structures (Fig. 2c), which correspond to the two open BISs at $k_y = 0$ and $-\pi$, respectively. Despite a trivial pattern along k_x with $k_y = -\pi$, the winding of the emergent dynamical spin-texture $\mathbf{g}(\mathbf{k})$ (in $x-z$ plane) along k_x with $k_y = 0$ measures the Chern number $C_1 = -1$ (Fig. 2d). Applying the dynamical classification to measuring topological states with high Chern numbers is straightforward and is found in Supplementary Material [41].

We further consider the application to 3D topological phases, whose hosting Hamiltonian reads $\mathcal{H}(\mathbf{k}) = \vec{h}(\mathbf{k}) \cdot \vec{\gamma}$, with $h_0(\mathbf{k}) = m_z - t_0 \sum_i \cos k_i$ and $h_i = t_{\text{so}} \sin k_i$ ($i = x, y, z$). Here we take that $\gamma_0 = \sigma_z \otimes \tau_x$, $\gamma_1 = \sigma_x \otimes \mathbb{1}$, $\gamma_2 = \sigma_y \otimes \mathbb{1}$ and $\gamma_3 = \sigma_z \otimes \tau_z$, where the Pauli matrices σ_i and τ_i may refer to the real- and pseudo-spin degrees of freedom (e.g., sublattices or orbitals). The Hamiltonian has a chiral symmetry defined by $\sigma_z \otimes \tau_y$, so it belongs to AIII class and is classified by 3D winding numbers in equilibrium theory [32–34]. The trivial phase corresponds to $|m_z| > 3t_0$, while the topological phases include three regions: (I) $t_0 < m_z < 3t_0$ with winding number $\nu_3 = -1$; (II) $-t_0 < m_z < t_0$ with $\nu_3 = 2$; and (III) $-3t_0 < m_z < -t_0$ with $\nu_3 = -1$. We consider the quench from $m_z \gg t_0$ to say phase I ($m_z = 1.3t_0$ and $t_{\text{so}} = 0.2t_0$), with the numerical results being partially presented in Fig. 3 (more is shown in Supplementary Material [41]). The BIS of the post-quench band is given in Fig. 3a. To extract the emergent dynamical field $\mathbf{g}(\mathbf{k})$, we plot the time-averaged spin polarizations $\langle \vec{\gamma} \rangle$ on two closed surfaces slightly inside (with $h_0 = -0.1t_0$) and outside (with $h_0 = 0.1t_0$) the BIS. The vector field $\mathbf{g}(\mathbf{k})$ can be approximately determined from the subtraction of $\langle \vec{\gamma} \rangle$ between the two surfaces. A few examples for $\langle \gamma_3 \rangle$ are given in Fig. 3 (b,c,d), similar for $\langle \gamma_{1,2} \rangle$ [41]. From these results we further determine the emergent dynamical field $\mathbf{g}(\mathbf{k})$ on the BIS, as illustrated with arrows in Fig. 3 (a), which gives a nonzero Chern number $C_1 = -1$ on the 2D BIS, leading to the 3D winding number $\nu_3 = -1$ of the post-quench 3D system.

While the above study is based on unitary quench dynamics, the dynamical classification can be generalized to the dissipative quantum dynamics at finite temperature. In the presence of dissipation, we expect that quantum dynamics should be nearly unitary within a short-time evolution after quench, while the dissipation effects shall dominate in the long-term evolution. Taking the 2D model as an example, we describe the dynamics by the Lindblad master equation [43, 44]

$$\frac{d}{dt} \rho_{\mathbf{k}} = -i [\mathcal{H}, \rho_{\mathbf{k}}] + \eta \left(\tilde{\sigma}_- \rho_{\mathbf{k}} \tilde{\sigma}_+ - \frac{1}{2} \{ \tilde{\sigma}_+ \tilde{\sigma}_-, \rho_{\mathbf{k}} \} \right) \quad (7)$$

with initial state being $\rho_{\mathbf{k}}(0) = f(E_+, T) |+, \mathbf{k}\rangle \langle +, \mathbf{k}| + f(E_-, T) |-, \mathbf{k}\rangle \langle -, \mathbf{k}|$. Here the distribution function $f(E, T) = [e^{(E-\mu)/k_B T} \pm 1]^{-1}$ if the system is simulated with fermions (for $+$) and bosons (for $-$), $|\pm, \mathbf{k}\rangle$ denote the eigenstates of the pre-quench Hamiltonian, the Pauli matrices $\tilde{\sigma}_\pm \equiv (\tilde{\sigma}_x \pm i\tilde{\sigma}_y)/2$ are defined in the eigenbasis of the post-quench Hamiltonian \mathcal{H} , and η is the decay rate. A numerical study with typical parameters is shown in Fig. 4. For a short-term evolution, we can see that the dissipative effect is negligible (nearly unitary), as demonstrated in Fig. 4a (gray area) and b. In this regime, the previous dynamical classification is well applicable to measure the location of BISs and the bulk topology

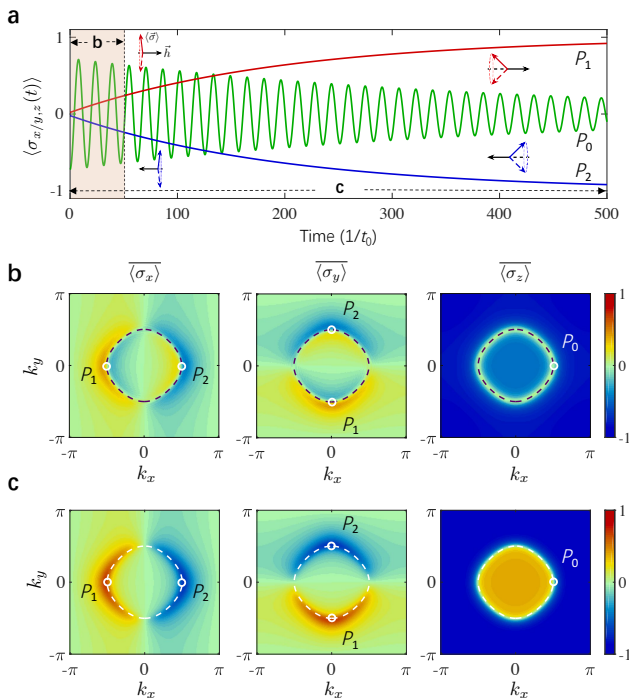


Figure 4: **Classifying topology via dissipative dynamics.** **a**, Post-quench dissipative dynamics of spin polarizations $\langle \sigma_{x,y}(t) \rangle$ (red and blue lines) for points $P_{1,2}$ and $\langle \sigma_z(t) \rangle$ (green line) for P_0 at finite temperature. Due to dissipation, the spin $\langle \vec{\sigma} \rangle$ gradually decays to the opposite direction of the precession axis $\vec{h}(\mathbf{k})$ (see insets). The BIS and topological patterns can be determined by time-averaged spin textures over a short period (see **b**) and a long period (see **c**), respectively. **b**, Time-averaged spin textures $\langle \sigma_{x,y,z} \rangle$ over a period of $50/t_0$, which resemble the results in Fig. 2a. The BIS is determined by $\langle \vec{\sigma} \rangle \simeq 0$ (black dashed line). **c**, Time-averaged spin textures $\langle \sigma_{x,y,z} \rangle$ on the BIS over a long term of $500/t_0$ directly reflect the SO field and thus the topological number. Here we take the temperature $k_B T = 10t_0$ and the decay rate $\eta = 0.005$ with other parameters the same as in Fig. 2a.

(Fig. 4b). Further, after a long-term evolution, the dissipation drives the occupation of Bloch states to approach the equilibrium result. In this case we can find that the spin-polarization $\langle \vec{\sigma}(\mathbf{k}) \rangle$ gradually points oppositely to the $\mathbf{h}_{\text{so}}(\mathbf{k})$ -direction on BISs of the post-quench system (Fig. 4a). Then the Chern number can be directly read out by the long-term spin texture $\langle \vec{\sigma}(\mathbf{k}) \rangle$, without the further adoption of $\vec{g}(\mathbf{k})$ for the classification [Fig. 4(a,c)].

Discussion and outlook.—The dynamical classification exhibits essential advantages for experimental investigation of topological quantum states. In particular, applying the classification theory proposed in this work to measuring 2D Chern insulators has been achieved in a very recent experiment [45], which confirms that the dynamical classification is of much higher precision in observing topological quantum physics, compared with the measurement strategies based on equilibrium classi-

fication. The advantages are rooted in two fundamental aspects. First, the bulk-surface (bulk-ring) duality uncovered here enables the classification of topology by lower-dimensional invariants, which largely simplifies the topological characterization. Moreover, the dynamical measurement by nature is insensitive to details of preparing the system. In particular, the system starts with deep trivial regime, with the initial state being independent of model details. Quenching it to topological regime induces quantum dynamics which exhibits resonant oscillations only on the BISs. The short-term unitary quench dynamics characterizing the topology of the post-quench system is insensitive to detrimental effects like the thermal effects, leading to high precision of measuring the full topological phase diagrams [45]. In comparison, measuring the topology of static phases necessitates the systems to be carefully initialized, with the quantum states being properly occupied. The preparation is intrinsically sensitive to non-ideal conditions including thermal effects, especially unsatisfactory in the regime close to phase boundaries [29]. The present dynamical classification provides fundamentally new approaches with high feasibility in exploring topological quantum physics.

Further, from the theoretical perspective, this work provides insights into developing dynamical classification for complete classes of topological quantum states. The dynamical classification theory established here covers quite a few different categories of the topological phases characterized by integer invariants, including the A, AIII, BDI, C, and D classes in the AZ ten-fold symmetry classification [32]. It is promising and of remarkable interests to generalize the current classification theory to all ten-fold categories [32–34], crystalline topological states, including the insulators and superconductors protected by lattice symmetries [35, 47], and even to the interacting topological states of fermions and bosons [20, 21]. We therefore expect that the present work can open a broad new direction to classify and detect topological quantum states by non-equilibrium quantum dynamics.

Acknowledgement.—This work was supported by the National Key R&D Program of China (2016YFA0301604), National Nature Science Foundation of China (under grants NO. 11674301 and No. 11761161003), and the Thousand-Young-Talent Program of China.

Methods

Numerical calculations.—The unitary dynamics after a sudden quench from $m_0 = m_{\text{in}}$ to m_{fi} is described by the time evolution operator $U(t) = \exp[-i\mathcal{H}(m_{\text{fi}})t]$, where $\mathcal{H}(m_{\text{fi}})$ is the Hamiltonian taking the post-quench parameter. The time-dependent density matrix is then $\rho(t) = U(t)\rho(0)U(t)^\dagger$. Here the initial state $\rho(0)$ is always chosen as the lowest energy band (or the lowest

two degenerate bands for 3D model) of the Hamiltonian $\mathcal{H}(m_{\text{in}})$. For fermions, we deal with it simply at zero temperature with the chemical potential being right in the energy gap. For bosons, we treat it at finite temperature. The temperature is well set so that the lowest band is sufficiently occupied with the chemical potential being determined by the particle density. The spin textures at time t are calculated by $\langle \sigma_j(t) \rangle = \text{Tr}[\rho(t)\sigma_j]$ ($j = x, y, z$), and the time average $\overline{\langle \sigma_j \rangle}$ is taken over a long enough period so that they approach the ones averaged over infinite time. The derivatives $\partial_{k_\perp} \overline{\langle \sigma_j \rangle}$ can be approximated by $\partial_{k_\perp} \overline{\langle \sigma_j \rangle} \simeq \left[\overline{\langle \sigma_j \rangle}_{k_\perp^>} - \overline{\langle \sigma_j \rangle}_{k_\perp^<} \right] / (k_\perp^> - k_\perp^<)$, where $k_\perp^>$ ($k_\perp^<$) is the momentum along the perpendicular direction in the region with $h_0 > 0$ ($h_0 < 0$) (see Fig. 1), and the dynamical field $\widetilde{g}_j(\mathbf{k}) = \mp \partial_{k_\perp} \overline{\langle \sigma_j \rangle}$, with the sign $-$ (or $+$) indicating the quench route from an initial trivial phase with $m_{\text{in}} \gg t_0$ (or $m_{\text{in}} \ll -t_0$). In the case of dissipative dynamics, the whole procedure is similar except that the density matrix is determined by the Lindblad equation.

* These authors contribute equally to this work.

- [1] K. v. Klitzing, G. Dorda, M. Pepper, New Method for High-Accuracy Determination of the Fine-Structure Constant Based on Quantized Hall Resistance. *Phys. Rev. Lett.* **45**, 494 (1980).
- [2] D. C. Tsui, H. L. Stormer, A. C. Gossard, Two-dimensional magnetotransport in the extreme quantum limit. *Phys. Rev. Lett.* **48**, 1559 (1982).
- [3] D. J. Thouless *et al.*, Quantized Hall Conductance in a Two-Dimensional Periodic Potential. *Phys. Rev. Lett.* **49**, 405 (1982).
- [4] X.-G. Wen, Topological orders in rigid states. *Int. J. of Mod. Phys. B* **4**, 239-271 (1990).
- [5] L. D. Landau, E. M. Lifshitz, and M. Pitaevskii, 1999, Statistical Physics (Butterworth-Heinemann, New York).
- [6] M. Z. Hasan and C. L. Kane, Topological insulators. *Rev. Mod. Phys.* **82**, 3045 (2010).
- [7] X. L. Qi and S. C. Zhang, Topological insulators and superconductors. *Rev. Mod. Phys.* **83**, 1057 (2011).
- [8] M. König *et al.*, Quantum Spin Hall Insulator State in HgTe Quantum Wells. *Science* **318**, 766 (2007).
- [9] D. Hsieh *et al.*, A topological Dirac insulator in a quantum spin Hall phase (experimental realization of a 3D Topological Insulator). *Nature* **452**, 970 (2008).
- [10] Y. Xia *et al.*, Observation of a large-gap topological-insulator class with a single Dirac cone on the surface. *Nat. Phys.* **5**, 398 (2009).
- [11] C.-Z. Chang *et al.*, Experimental Observation of the Quantum Anomalous Hall Effect in a Magnetic Topological Insulator. *Science* **340**, 167 (2013).
- [12] S.-Y. Xu *et al.*, Discovery of a Weyl Fermion Semimetal and Topological Fermi Arcs. *Science* **349**, 613 (2015).
- [13] B. Q. Lv *et al.*, Experimental discovery of weyl semimetal TaAs. *Phys. Rev. X* **5**, 31013 (2015).
- [14] B. Bradlyn *et al.*, *Nature* **547**, 298 (2017).
- [15] A. Kitaev, Unpaired Majorana fermions in quantum wires. *Physics-Usppekhi* **44**, 131 (2001).
- [16] N. Read and D. Green, Paired states of fermions in two dimensions with breaking of parity and time-reversal symmetries and the fractional quantum Hall effect. *Phys. Rev. B* **61**, 10267 (2000).
- [17] J. Alicea, New directions in the pursuit of Majorana fermions in solid state systems. *Rep. Prog. Phys.* **75**, 76501 (2012).
- [18] S. R. Elliott, M. Franz, Colloquium: Majorana Fermions in nuclear, particle and solid-state physics. *Rev. Mod. Phys.* **87**, 137 (2014).
- [19] M. Sato and Y. Ando, Topological superconductors: a review. *Rep. Prog. Phys.* **80**, 076501 (2017).
- [20] X. Chen *et al.*, Symmetry-Protected Topological Orders in Interacting Bosonic Systems. *Science* **338**, 1604 (2012).
- [21] X. Chen *et al.*, Symmetry protected topological orders and the group cohomology of their symmetry group. *Phys. Rev. B* **87**, 155114 (2013).
- [22] W. P. Su *et al.*, Soliton excitations in polyacetylene. *Phys. Rev. B* **22**, 2099 (1980).
- [23] M. Atala *et al.*, Direct Measurement of the Zak phase in Topological Bloch Bands. *Nat. Phys.* **9**, 795 (2012).
- [24] X.-J. Liu, Z.-X. Liu, and M. Cheng, Manipulating Topological Edge Spins in a One-Dimensional Optical Lattice. *Phys. Rev. Lett.* **110**, 076401 (2013).
- [25] B. Song, L. Zhang, C. He, T. F. J. Poon, E. H. H. Jijev, S. Zhang, X.-J. Liu, and G.-B. Jo, Observation of symmetry-protected topological band with ultracold fermions. *Science Advances* **4**, eaao4748 (2018).
- [26] G. Jotzu *et al.*, Experimental realization of the topological Haldane model with ultracold fermions. *Nature* **515**, 237-240 (2014).
- [27] M. Aidelsburger *et al.*, Measuring the Chern number of Hofstadter bands with ultracold bosonic atoms. *Nat. Phys.* **11**, 162-166 (2015).
- [28] Z. Wu *et al.*, Realization of two-dimensional spin-orbit coupling for Bose-Einstein condensates. *Science* **354**, 82 (2016).
- [29] W. Sun *et al.*, Long-lived 2D Spin-Orbit coupled Topological Bose Gas. arXiv:1710.00717.
- [30] M. Tarnowski *et al.*, Characterizing topology by dynamics: Chern number from linking number. arXiv: 1709.01046.
- [31] C. Wang *et al.*, Scheme to Measure the Topological Number of a Chern Insulator from Quench Dynamics. *Phys. Rev. Lett.* **118**, 185701 (2017).
- [32] A. Altland and Martin R. Zirnbauer, Nonstandard symmetry classes in mesoscopic normal-superconducting hybrid structures. *Phys. Rev. B* **55**, 1142 (1997).
- [33] A. P. Schnyder *et al.*, Classification of topological insulators and superconductors in three spatial dimensions. *Phys. Rev. B* **78**, 195125 (2008).
- [34] A. Kitaev, Periodic table for topological insulators and superconductors. *AIP Conference Proceedings* **1134**, 22 (2009).
- [35] C.-K. Chiu *et al.*, Classification of topological quantum matter with symmetries. *Rev. Mod. Phys.* **88**, 035005 (2016).
- [36] T. Morimoto *et al.*, Topological classification with additional symmetries from Clifford algebras. *Phys. Rev. B* **88**, 125129 (2013).
- [37] C.-K. Chiu *et al.*, Classification of topological insulators and superconductors in the presence of reflection symmetry. *Phys. Rev. B* **88**, 075142 (2013).

- [38] F. D. M. Haldane, Model for a Quantum Hall Effect without Landau Levels: Condensed-Matter Realization of the “Parity Anomaly”. *Phys. Rev. Lett.* **61**, 2015 (1988).
- [39] G. Volovik, *The universe in a helium droplet* (Clarendon Press, 2003).
- [40] S. C. Zhang and J. Hu, A four-dimensional generalization of the quantum Hall effect. *Science*, **294**, 823-828 (2001).
- [41] See Supplementary Material for more details.
- [42] X.-J. Liu, K. T. Law, and T. K. Ng, Realization of 2D Spin-Orbit Interaction and Exotic Topological Orders in Cold Atoms. *Phys. Rev. Lett.* **112**, 086401 (2014).
- [43] G. Lindblad, On the generators of quantum dynamical semigroups. *Commun. Math. Phys.* **48**, 119-130 (1976).
- [44] Y. Hu, P. Zoller, and J. C. Budich, Dynamical buildup of a quantized hall response from nontopological states. *Phys. Rev. Lett.* **117**, 126803 (2016).
- [45] W. Sun *et al.*, Uncovering topology by quenching dynamics. Manuscript to appear.
- [46] K. Shiozaki *et al.*, Topology of crystalline insulators and superconductors. *Phys. Rev. B* **90**, 165114 (2014).
- [47] R. -J. Slager *et al.*, The space group classification of topological band-insulators. *Nat. Phys.* **9**, 98 (2013).
- [48] C. Chan *et al.*, Generic Theory for Majorana Zero Modes in 2D Superconductors. *Phys. Rev. Lett.* **119**, 047001 (2017).

SUPPLEMENTARY MATERIAL

I. Characterizing d D Topological Phases by $(d-1)$ D Invariants

A. The generic model

We consider the generic d -dimensional (d D) gapped topological phases, which can be insulators or superconductors. To capture the essential topological features, the basic Hamiltonian can be written in terms of the elementary representation of the Clifford algebra [36, 37] as

$$\mathcal{H}(\mathbf{k}) = \vec{h}(\mathbf{k}) \cdot \vec{\gamma} = h_0(\mathbf{k})\gamma_0 + \sum_{i=1}^d h_i(\mathbf{k})\gamma_i, \quad (\text{S1})$$

where the matrices $\vec{\gamma}$ define a (pseudo)spin and obey the Clifford algebra $\{\gamma_i, \gamma_j\} = 2\delta_{ij}\mathbb{1}$ for $i, j = 0, 1, \dots, d$ (see Tab. I for more properties). The $(d+1)$ D vector field $\vec{h}(\mathbf{k})$ describes an effective Zeeman field depending on the Bloch momentum \mathbf{k} in the Brillouin zone (BZ). Here the elementary representations of the Clifford algebra (i.e., Clifford matrices for brevity) are of dimensionality $n_d = 2^{d/2}$ (or $2^{(d+1)/2}$) if d is even (or odd), and involve the minimal bands to open a topological gap for the d D topological phase. In one and two dimensions, for example, the Clifford matrices γ_i simply reduce to the Pauli matrices, and the basic Hamiltonian involves two bands for the topological states, e.g., the famous Su-Schrieffer-Heeger (SSH) model [22, 35] in 1D BDI class [24] and the Haldane model [38] for Chern insulator in 2D A class. Similarly, the Clifford matrices γ_i take the Dirac forms for the 3D and 4D phases, and a fully gapped topological phase involves at least four bands, such as the 3D class DIII $^3\text{He-B}$ [35, 39] and the 4D quantum Hall effect [40]. The results in this work are not dependent on the above minimal Hamiltonian written in terms of basic representation, but are valid for generic many-band systems. For a general multiband model of d D topological phases, the basic Hamiltonian can be written down locally for those bands relevant to topology, and ‘‘gluing’’ all these Hamiltonians smoothly will give the topology of the total system (for details, see later).

Here we focus on systems classified by \mathbb{Z} in the Altland-Zirnbauer symmetry classes [33–35], which include classes AIII, BDI, CII in 1D, classes A, D, C in 2D, classes AIII, DIII, CI in 3D, and so on. These classes can describe the topological insulators or superconductors and are characterized by the winding number in odd dimensions or Chern number in even dimensions [35, 46], which characterizes the winding of the map $\mathbf{n}(\mathbf{k}) = \vec{h}/|\vec{h}|$ from a d D torus T^d to the d D spherical surface S^d . By definition, identifying the topological invariants requires the d -dimensional bulk information. However, as pointed out in the main text and will be proved here, the d -dimensional topology can be characterized by a $(d-1)$ -dimensional invariant defined on the so-called ‘‘band-inversion surfaces’’ (BISs).

dimension d	Clifford matrices	chiral matrix	$\text{Tr}[\gamma \prod_{i=0}^d \gamma_i]$ or $\text{Tr}[\prod_{i=0}^d \gamma_i]$
1	$\gamma_0^{(1)} = \sigma_x, \gamma_1^{(1)} = \sigma_y$	$\gamma^{(1)} = \text{i}\sigma_x\sigma_y$	-2i
2	$\gamma_0^{(2)} = \gamma_0^{(1)}, \gamma_1^{(2)} = \gamma_1^{(1)}, \gamma_2^{(2)} = \gamma^{(1)}$	–	-2i
$2n-1$	$\gamma_i^{(2n-1)} = \gamma_i^{(2n-3)} \otimes \sigma_z$ for $i = 0, 1, \dots, 2n-3$, $\gamma_{2n-2}^{(2n-1)} = \mathbb{1} \otimes \sigma_x, \gamma_{2n-1}^{(2n-1)} = \mathbb{1} \otimes \sigma_y$	$\gamma^{(2n-1)} = -\gamma_{2n-3} \otimes \sigma_z$	$-2\text{i} \text{Tr}[\gamma^{(2n-3)} \prod_{i=0}^{2n-3} \gamma_i^{(2n-3)}]$ $= (-2\text{i})^n$
$2n$	$\gamma_i^{(2n)} = \gamma_i^{(2n-1)}$ for $i = 0, 1, \dots, 2n-1$, $\gamma_{2n}^{(2n)} = \gamma^{(2n-1)}$	–	$(-2\text{i})^n$

Table I: **Construction of Clifford matrices and their trace property.** Here $\sigma_{x,y,z}$ are Pauli matrices. For odd dimensions $d = 2n-1$, one can define a chiral matrix $\gamma = (\text{i})^n \prod_{i=0}^{2n-1} \gamma_i$, which satisfies $\gamma^\dagger = \gamma$, $\gamma^2 = \mathbb{1}$ and $\{\gamma, \gamma_i\} = 0$. These Clifford matrices have the trace property $\text{Tr}[\gamma\gamma_i\gamma_j \dots \gamma_s\gamma_t] = (-2\text{i})^n \epsilon^{ij\dots st}$ for odd dimensions, and $\text{Tr}[\gamma_i\gamma_j \dots \gamma_s\gamma_t] = (-2\text{i})^n \epsilon^{ij\dots st}$ for even dimensions, which can be obtained by induction (the last column).

B. The band-inversion surfaces

For the basic Hamiltonian (S1), to facilitate the further discussion and without loss of the generality, we choose that $h_0(\mathbf{k})$ characterizes the band structure and ‘dispersion’ of the n_d decoupled bands. Accordingly, the remaining

d -components $h_{i \neq 0}(\mathbf{k})$ ($i = 1, 2, \dots, d$) depict the coupling between different bands, mimicking the spin-orbit (SO) coupling. We denote by these components the SO field $\mathbf{h}_{\text{so}}(\mathbf{k}) \equiv (h_1, \dots, h_d)$. For topological superconductors, the SO field defined here corresponds to the superconducting pairings. Note that one can pick up any component from $\vec{h}(\mathbf{k})$ as $h_0(\mathbf{k})$, and take the remaining components as the SO field, which will be exemplified later.

For dD gapped topological phases, in the absence of the SO field, the band crossing occurs for the n_d decoupled bands and the system becomes gapless on a $(d-1)D$ surface if $h_0(\mathbf{k}) = 0$ at certain momentum points of the BZ, which is dubbed band-inversion surface (BIS), i.e.,

$$\text{BIS} \equiv \{\mathbf{k} | h_0(\mathbf{k}) = 0\}. \quad (\text{S2})$$

In particular, the BIS coincides with the Fermi surface for topological superconductors. Generically, there can be multiple BISs in the BZ, and some of them can be open (Fig. S1a-c). Here, for convenience, we denote by \mathcal{V}_{BIS} the region enclosed by BISs with $h_0(\mathbf{k}) < 0$, and decompose the momentum \mathbf{k} into $(k_{\perp}, \mathbf{k}_{\parallel})$ with k_{\perp} being perpendicular to the BIS and pointing to the region $\bar{\mathcal{V}}_{\text{BIS}}$ with $h_0(\mathbf{k}) > 0$.

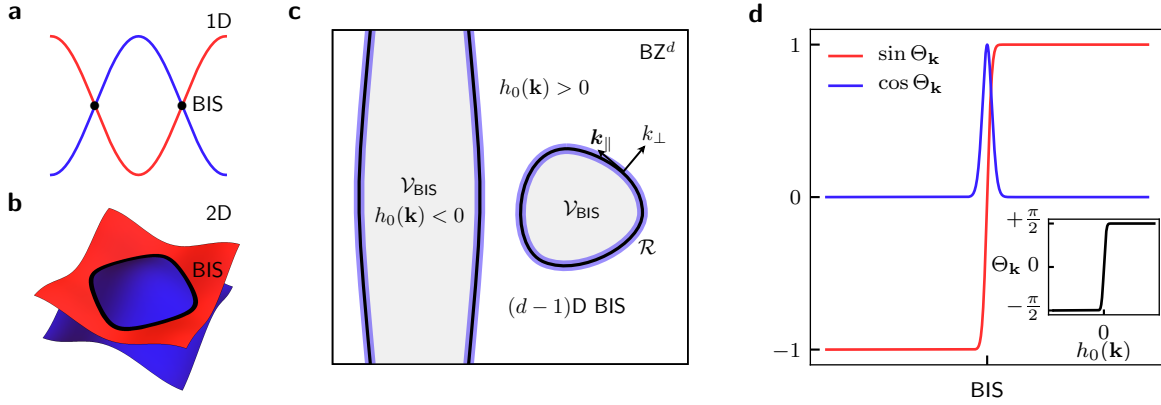


Figure S1: **The schematic diagram of BISs and the deformation technique.** **a-b**, BISs in 1D and 2D. In 1D, the BIS (black dots) composes of discrete points **(a)**, and becomes a 1D closed curve (the black ring) in 2D **(b)**. **c**, $(d-1)D$ BISs in dD BZ. Here \mathcal{V}_{BIS} denotes the region enclosed by BIS with $h_0(\mathbf{k}) < 0$ (gray). The momentum \mathbf{k} is decomposed into $(k_{\perp}, \mathbf{k}_{\parallel})$ with k_{\perp} perpendicular to the contour of $h_0(\mathbf{k})$ and pointing to the side $\bar{\mathcal{V}}_{\text{BIS}}$ with $h_0(\mathbf{k}) > 0$. **d**, The function $\sin \Theta_{\mathbf{k}}$ (red) and $\cos \Theta_{\mathbf{k}}$ (blue) used in the deformed Hamiltonian (S3). The insert shows the function $\Theta_{\mathbf{k}}$. The region with non-zero SO field ($\cos \Theta_{\mathbf{k}}$) is denoted by \mathcal{R} (blue) in **c**.

C. Bulk-surface duality: the $(d-1)D$ topological invariant on the BISs

Note that the SO field gaps out the BISs. We shall show that the SO field on the BISs determines the topology uniquely, for which the dD bulk topology can be characterized by a $(d-1)D$ invariant defined on the BISs. To prove it, we shall take advantage of the fact that the topology remains unchanged under any continuous deformation that does not close the gap [48]. Therefore, we can keep the SO field only in the region near the BISs but turn it off elsewhere, which results in the following deformed Hamiltonian

$$\mathcal{H}(\mathbf{k}) \rightarrow \vec{h}'(\mathbf{k}) \cdot \vec{\gamma} = \sin \Theta_{\mathbf{k}} \gamma_0 + \cos \Theta_{\mathbf{k}} \sum_{i=1}^d \hat{h}_{\text{so},i}(\mathbf{k}) \gamma_i, \quad (\text{S3})$$

where $\hat{h}_{\text{so}}(\mathbf{k}) \equiv \mathbf{h}_{\text{so}}(\mathbf{k}) / |\mathbf{h}_{\text{so}}(\mathbf{k})|$ denotes the unit SO field. Here $\Theta_{\mathbf{k}} \in [-\pi/2, \pi/2]$ is a smooth and monotonic function of $h_0(\mathbf{k})$, which approaches the step function and maps $h_0(\mathbf{k})$ to $\pm\pi/2$ if $h_0(\mathbf{k}) \gtrless 0$ or to 0 if $h_0(\mathbf{k}) = 0$, see Fig. S1d. For example, it can be chosen as the error function $\pi \text{erf}(\xi h_0(\mathbf{k})) / 2$ with $\xi \rightarrow \infty$. On the other hand, the SO field with pre-factor $\cos \Theta_{\mathbf{k}}$ is truncated to the region near the BISs. It is noteworthy that this deformation keeps the information of BISs including the SO field on it, and the deformed Hamiltonian has been normalized.

In the following we shall show explicitly a bulk-surface duality that classifying the topological phases with integer invariants, the d D winding number (or Chern number), can be mapped to the classification of topology, by $(d-1)$ D Chern number (or winding number), measured from the SO field on the $(d-1)$ D BISs:

$$w_{d-1} = \sum_j \frac{\Gamma(d/2)}{2\pi^{d/2}} \frac{1}{(d-1)!} \int_{\text{BIS}_j} \hat{\mathbf{h}}_{\text{so}} (d\hat{\mathbf{h}}_{\text{so}})^{d-1}, \quad (\text{S4})$$

where $\Gamma(x)$ is the Gamma function, $\hat{\mathbf{h}}_{\text{so}}(d\hat{\mathbf{h}}_{\text{so}})^{d-1} \equiv \epsilon^{i_1 i_2 \dots i_d} \hat{h}_{\text{so}, i_1} d\hat{h}_{\text{so}, i_2} \wedge \dots \wedge d\hat{h}_{\text{so}, i_d}$, with $\epsilon^{i_1 i_2 \dots i_d}$ the fully anti-symmetric tensor and $i_{1,2,\dots,d} \in \{1, 2, \dots, d\}$, and ‘d’ denotes the exterior derivative. The integral in the right hand side characterizes the mapping from BISs to the $(d-1)$ D spherical surface S^{d-1} of which $\hat{\mathbf{h}}_{\text{so}}(\mathbf{k})$ are elements. Intuitively, it counts the times that the SO field $\hat{\mathbf{h}}_{\text{so}}(\mathbf{k})$ covers the $(d-1)$ D spherical surface S^{d-1} as the momentum \mathbf{k} runs over all BISs. As we shall see later, the above formula can also be written as $w_{d-1} = \sum_{i \in \mathcal{V}_{\text{BIS}}} \mathcal{C}_i$, with \mathcal{C}_i denoting the total topological charge characterized by the vanishing SO field with $\mathbf{h}_{\text{so}}(\mathbf{k}) = 0$ in the patch of volume \mathcal{V}_{BIS} enclosed by the i -th BIS.

The proof for the generic theorem given in Eq. (S4) is highly nontrivial and relies on brutal force. To get the insights, we shall first introduce the proof for the simple cases with 1D, 2D, and 3D topological phases. Our proof will be based on the deformed Hamiltonian (S3), and the winding number or Chern number can be defined using the normalized Hamiltonian [46].

1. 1D topological phases characterized by the winding number

We start with the 1D topological phases, which are the simplest cases, with the basic Hamiltonian for the topology being two-band models. Accordingly, the Clifford matrices γ_i are generated by the Pauli matrices, $\gamma_{i=0,1} \in \{\sigma_x, \sigma_y, \sigma_z\}$. The Hamiltonian $\mathcal{H}(k)$ has chiral symmetry $\gamma = i\gamma_0\gamma_1$ and is characterized by the 1D winding number:

$$\begin{aligned} \nu_1 &\equiv \frac{1}{4\pi i} \int_{\text{BZ}} \text{Tr}[\gamma \mathcal{H} d\mathcal{H}] \\ &= \frac{1}{4\pi i} \int_{\text{BZ}} dk (h'_0 \partial_k h'_1 - h'_1 \partial_k h'_0) \text{Tr}[\gamma \gamma_0 \gamma_1], \end{aligned} \quad (\text{S5})$$

here we have used the fact $\sum_{i=0}^d h_i'^2 = 1$ for the normalized Hamiltonian (S3). With the deformed Hamiltonian and the trace property of Clifford matrices $\text{Tr}[\gamma_i \gamma_j] = -2i\epsilon^{ij}$, the winding number can be further written as

$$\begin{aligned} \nu_1 &= \frac{1}{2\pi} \int_{\text{BZ}} d\Theta_k \hat{h}_{\text{so}} \\ &= \frac{1}{2} \sum_{\text{BIS}_j} [\text{sgn}(h_{1,R_j}) - \text{sgn}(h_{1,L_j})], \end{aligned} \quad (\text{S6})$$

where the unit SO field $\hat{h}_{\text{so}} = \text{sgn}(h_1)$ for 1D, with $\text{sgn}(x)$ being the sign function, and the BISs become discrete points (see Fig. S1a), with the left hand and right hand points of the j -th BIS being denoted as L_j and R_j , respectively. Thus the right hand side of the above formula denotes a zero-dimensional invariant (0-th Chern number). Note that the region \mathcal{V}_{BIS} enclosed by each BIS refers to that with $h_0(k) < 0$. The integral of Θ_k must become $+\pi$ at the right-hand (R_j) and $-\pi$ at the left-hand (L_j) point of the j -th BIS, which results in the prefactors of $\text{sgn}(h_{1,R_j})$ and $\text{sgn}(h_{1,L_j})$, respectively. For the case with only a single BIS, the equation (S6) gives the result with a simple picture that the system is topologically nontrivial when the SO field has opposite signs at the R and L points of BIS, otherwise it is trivial.

As an example, we consider the 1D model of the AIII class in the main text, which has the Hamiltonian $\mathcal{H}(k) = \vec{h}(k) \cdot \vec{\sigma}$ with $h_x = t_{\text{so}} \sin k \equiv h_{\text{so}}$, $h_y = 0$ and $h_z = m_z - t_0 \cos k \equiv h_0$. Here $t_0 > 0$ and $t_{\text{so}} > 0$ denote the nearest-neighbor spin-conserved and spin-flipped hopping coefficients, m_z is the effective magnetization. When $|m_z| > t_0$, this model is trivial as there is no BISs. On the other hand, the BIS is determined by $k_{\text{BIS}} = \pm \arccos m_z/t_0$ when $|m_z| < t_0$. It is easy to check that $h_{\text{so}} > 0$ for the right hand point of the BIS and $h_{\text{so}} < 0$ for the left hand point, which indicates the winding number $\nu_1 = 1$.

2. 2D topological phases characterized by the first Chern number

For the 2D topological phases, a two-band model can be formulated with three Pauli matrices that $\gamma_i \in \{\sigma_x, \sigma_y, \sigma_z\}$ for $i = 0, 1, 2$. Accordingly, the topology of the phase is characterized by the first Chern number

$$\text{Ch}_1 = -\frac{i}{16\pi} \int_{\text{BZ}} \text{Tr}[\mathcal{H}(\text{d}\mathcal{H})^2]. \quad (\text{S7})$$

The trace is taken in the spin space. Using the relation $\mathcal{H}(\text{d}\mathcal{H})^2 = \sum_i \sum_{j \neq k} h'_i \text{d}h'_j \wedge \text{d}h'_k \gamma_i \gamma_j \gamma_k$ and the trace property $\text{Tr}[\gamma_i \gamma_j \gamma_k] = -2i\epsilon^{ijk}$, where the Levi-Civita tensor and the wedge are both anti-symmetric, we further obtain the Chern number that

$$\text{Ch}_1 = -\frac{1}{4\pi} \int_{\text{BZ}} \text{d}^2\mathbf{k} \cdot (h'_0 \nabla h'_1 \times \nabla h'_2 - h'_1 \nabla h'_0 \times \nabla h'_2 + h'_2 \nabla h'_0 \times \nabla h'_1). \quad (\text{S8})$$

From the deformed Hamiltonian (S3) we obtain that

$$\begin{aligned} h'_0 \nabla h'_1 \times \nabla h'_2 &= \sin \Theta_{\mathbf{k}} \cos^2 \Theta_{\mathbf{k}} \nabla \hat{h}_{\text{so},1} \times \nabla \hat{h}_{\text{so},2} \\ &\quad - \sin^2 \Theta_{\mathbf{k}} \cos \Theta_{\mathbf{k}} \nabla \Theta_{\mathbf{k}} \times (\hat{h}_{\text{so},1} \nabla \hat{h}_{\text{so},2} - \hat{h}_{\text{so},2} \nabla \hat{h}_{\text{so},1}), \\ h'_i \nabla h'_0 \times \nabla h'_j &= \cos^3 \Theta_{\mathbf{k}} \nabla \Theta_{\mathbf{k}} \times \hat{h}_{\text{so},i} \nabla \hat{h}_{\text{so},j}. \end{aligned}$$

With the above results the Chern number is recast into

$$\text{Ch}_1 = -\frac{1}{4\pi} \int_{\text{BZ}} \text{d}^2\mathbf{k} \cdot [\sin \Theta_{\mathbf{k}} \cos^2 \Theta_{\mathbf{k}} \nabla \hat{h}_{\text{so},1} \times \nabla \hat{h}_{\text{so},2} - \cos \Theta_{\mathbf{k}} \nabla \Theta_{\mathbf{k}} \times (\hat{h}_{\text{so},1} \nabla \hat{h}_{\text{so},2} - \hat{h}_{\text{so},2} \nabla \hat{h}_{\text{so},1})]. \quad (\text{S9})$$

To simplify the above formula, we can choose a special configuration of the $\Theta_{\mathbf{k}}$ function, while the final result is independent of the choice of $\Theta_{\mathbf{k}}$. For this we let the SO field ($\propto \cos \Theta_{\mathbf{k}}$) for the deformed Hamiltonian be truncated to the BISs ($\sin \Theta_{\mathbf{k}} = 0$) by taking $\Theta_{\mathbf{k}}$ to approach the step function. Then the contribution from the first term vanishes. On the other hand, $\nabla \Theta_{\mathbf{k}}$ tends to a delta function, and the second term will contribute to the Chern number. Therefore, the whole integral can be reduced to that for the second term over the region \mathcal{R} with non-zero $\nabla \Theta_{\mathbf{k}}$ (see Fig. S1c-d):

$$\begin{aligned} \text{Ch}_1 &= \frac{1}{4\pi} \int_{\mathcal{R}} \text{d}^2\mathbf{k} \cdot \cos \Theta_{\mathbf{k}} \nabla \Theta_{\mathbf{k}} \times (\hat{h}_{\text{so},1} \nabla \hat{h}_{\text{so},2} - \hat{h}_{\text{so},2} \nabla \hat{h}_{\text{so},1}) \\ &= \frac{1}{4\pi} \int_{-\pi/2}^{\pi/2} \text{d}\Theta_{k_{\perp}} \cos \Theta_{k_{\perp}} \sum_j \oint_{\text{BIS}_j} \text{d}k_{\parallel} (\hat{z} \times \hat{n}_{\perp}) \cdot (\hat{h}_{\text{so},1} \nabla \hat{h}_{\text{so},2} - \hat{h}_{\text{so},2} \nabla \hat{h}_{\text{so},1}) \\ &= \sum_j \frac{1}{2\pi} \oint_{\text{BIS}_j} \text{d}\hat{\ell} \cdot (\hat{h}_{\text{so},1} \nabla \hat{h}_{\text{so},2} - \hat{h}_{\text{so},2} \nabla \hat{h}_{\text{so},1}) \\ &= \sum_j \frac{1}{2\pi} \epsilon^{mn} \oint_{\text{BIS}_j} \text{d}\hat{\ell} \cdot \hat{h}_{\text{so},m} \nabla \hat{h}_{\text{so},n}, \end{aligned} \quad (\text{S10})$$

where we have decomposed the momentum \mathbf{k} into $(k_{\perp}, k_{\parallel})$ in the second line, with k_{\perp} perpendicular to the BIS and pointing to the side \mathcal{V}_{BIS} with $h_0(\mathbf{k}) > 0$ (see Fig. S1c), and $m, n = 1, 2$. From the last line of the above formula we know that the final result is independent of the function $\Theta_{\mathbf{k}}$. Equation (S10) shows that the Chern number in the bulk reduces to the 1D winding of the SO field $\hat{\mathbf{h}}_{\text{so}}$ on the 1D BISs (band inversion rings). The integral $\sum_j \frac{1}{2\pi} \epsilon^{\alpha\beta} \oint_{\text{BIS}_j} \text{d}\hat{\ell} \cdot \hat{h}_{\text{so},\alpha} \nabla \hat{h}_{\text{so},\beta}$ is performed on the 1D BISs, with the positive direction defined so that the closed integral paths denote the boundary of the vector area \mathcal{V}_{BIS} . The 1D winding number then counts the total vorticity of the SO field at the degenerate points, i.e., the total topological charge of the 2D Dirac points, characterized by $\hat{\mathbf{h}}_{\text{so}} = 0$ within \mathcal{V}_{BIS} . The above result implies that, the first Chern number is simply given by the total topological charge of the SO field in the region enclosed by BISs, namely, in the \mathcal{V}_{BIS} with $h_0(\mathbf{k}) < 0$.

Here we take the Chern insulator in the main text as an example, whose Hamiltonian can be written as $\mathcal{H}(\mathbf{k}) = \vec{h}(\mathbf{k}) \cdot \vec{\sigma}$ with $\vec{h}(\mathbf{k}) = (t_{\text{so}} \sin k_x, t_{\text{so}} \sin k_y, m_z - t_0 \cos k_x - t_0 \cos k_y)$. Without loss of the generality, we can decompose the vector field \vec{h} into $h_0 \equiv h_z$ and $\mathbf{h}_{\text{so}} \equiv (h_y, h_x)$. When $m_z > 2$, there is no BISs and the system is trivial. When $0 < m_z < 2$, a topological charge -1 located at $\mathbf{k} = 0$ in \mathcal{V}_{BIS} is enclosed by the BIS, and gives the Chern number

$\text{Ch}_1 = -1$, see Fig. S2a. Furthermore, another two topological charges $+1$ at $(0, \pi)$ and $(\pi, 0)$ are also included when $-2 < m_z < 0$, which renders the Chern number being changed to $1 + 1 - 1 = +1$. Finally, when $m_z < -2$, the region \mathcal{V}_{BIS} equals the whole BZ, and all the four Dirac points $\{(0, 0), (\pi, \pi), (0, \pi), (\pi, 0)\}$ should be considered and contribute a trivial total topological charge ($1 + 1 - 1 - 1 = 0$).

On the other hand, one can also choose that $h_0 \equiv t_{\text{so}} \sin k_x$, in which case \mathcal{V}_{BIS} with $h_0(\mathbf{k}) < 0$ corresponds to the region with $-\pi < k_x < 0$, and then the SO field is $\mathbf{h}_{\text{so}} \equiv (h_z, h_y)$. A pair of topological charges with opposite signs, located at $\mathbf{k} = (\pm \arccos[(m_z + 1)/t_0], \pi)$ for $-2 < m_z < 0$ and at $\mathbf{k} = (\pm \arccos[(m_z - 1)/t_0], 0)$ for $0 < m_z < 2$, will be created from vacuum, moves and finally annihilates, as m_z varies from $-\infty$ to $+\infty$. Only one of the two charges is located in \mathcal{V}_{BIS} and enclosed by the BIS, giving the Chern number $C_1 = +1$ (for $-2 < m_z < 0$) or $C_1 = -1$ (for $0 < m_z < 2$) [see Fig. S2b]. The results are clearly consistent with those given above by choosing $h_0 = h_z(\mathbf{k})$.

3. 3D topological phases characterized by the winding number

For 3D topological phases, the minimal Hamiltonian involves four bands, and the Clifford matrices take the Dirac forms. The Hamiltonian has chiral symmetry $\gamma = -\prod_{i=0}^3 \gamma_i$ and is characterized by the 3D winding number

$$\nu_3 = \frac{1}{48\pi^2} \int_{\text{BZ}} \text{Tr}[\gamma \mathcal{H} (d\mathcal{H})^3]. \quad (\text{S11})$$

Similar to the 2D case, the relation $\mathcal{H} (d\mathcal{H})^3 = \sum_i \sum_{j \neq s \neq t} h'_i dh'_j \wedge dh'_s \wedge dh'_t$ and the trace gives $\text{Tr}[\gamma \gamma_i \gamma_j \gamma_s \gamma_t] = -4\epsilon^{ijst}$, with which the winding number takes the following explicit form

$$\nu_3 = -\frac{1}{2\pi^2} \int_{\text{BZ}} d^3\mathbf{k} \left\{ h'_0 \nabla h'_1 \cdot (\nabla h'_2 \times \nabla h'_3) - \nabla h'_0 \cdot [h'_1 \nabla h'_2 \times \nabla h'_3 - h'_2 \nabla h'_1 \times \nabla h'_3 + h'_3 \nabla h'_1 \times \nabla h'_2] \right\}. \quad (\text{S12})$$

From the deformed Hamiltonian (S3), the integrand in the winding number can be simplified by

$$\begin{aligned} h'_0 \nabla h'_1 \cdot (\nabla h'_2 \times \nabla h'_3) &= \sin \Theta_{\mathbf{k}} \cos^3 \Theta_{\mathbf{k}} \nabla \hat{h}_{\text{so},1} \cdot (\nabla \hat{h}_{\text{so},2} \times \nabla \hat{h}_{\text{so},3}) \\ &\quad - \sin^2 \Theta_{\mathbf{k}} \cos^2 \Theta_{\mathbf{k}} \Theta_{\mathbf{k}} \nabla \Theta_{\mathbf{k}} \cdot (\hat{h}_{\text{so},1} \nabla \hat{h}_{\text{so},2} \times \nabla \hat{h}_{\text{so},3} \\ &\quad - \hat{h}_{\text{so},2} \nabla \hat{h}_{\text{so},1} \times \nabla \hat{h}_{\text{so},3} + \hat{h}_{\text{so},3} \nabla \hat{h}_{\text{so},1} \times \nabla \hat{h}_{\text{so},2}), \\ h'_i \nabla h'_0 \cdot (\nabla h'_j \times \nabla h'_k) &= \cos^4 \Theta_{\mathbf{k}} \nabla \Theta_{\mathbf{k}} \cdot (\hat{h}_{\text{so},i} \nabla \hat{h}_{\text{so},j} \times \nabla \hat{h}_{\text{so},k}). \end{aligned}$$

Similar to the derivation done for the 2D phase, we take a special configuration that $\Theta_{\mathbf{k}}$ approaches the step function. The computation of the winding number finally reduces to the integral on the BISs, given by

$$\begin{aligned} \nu_3 &= \frac{1}{2\pi^2} \int_{\mathcal{R}} d^3\mathbf{k} \cos^2 \Theta_{\mathbf{k}} \nabla \Theta_{\mathbf{k}} \cdot [\hat{h}_{\text{so},1} \nabla \hat{h}_{\text{so},2} \times \nabla \hat{h}_{\text{so},3} - \hat{h}_{\text{so},2} \nabla \hat{h}_{\text{so},1} \times \nabla \hat{h}_{\text{so},3} + \hat{h}_{\text{so},3} \nabla \hat{h}_{\text{so},1} \times \nabla \hat{h}_{\text{so},2}] \\ &= \frac{1}{2\pi^2} \int_{-\pi/2}^{\pi/2} d\Theta_{k_{\perp}} \cos^2 \Theta_{k_{\perp}} \sum_j \int_{\text{BIS}_j} d^2\mathbf{k}_{\parallel} \cdot [\hat{h}_{\text{so},1} \nabla \hat{h}_{\text{so},2} \times \nabla \hat{h}_{\text{so},3} - \hat{h}_{\text{so},2} \nabla \hat{h}_{\text{so},1} \times \nabla \hat{h}_{\text{so},3} + \hat{h}_{\text{so},3} \nabla \hat{h}_{\text{so},1} \times \nabla \hat{h}_{\text{so},2}] \\ &= \sum_j \frac{1}{4\pi} \int_{\text{BIS}_j} d^2\mathbf{k}_{\parallel} \cdot [\hat{h}_{\text{so},1} \nabla \hat{h}_{\text{so},2} \times \nabla \hat{h}_{\text{so},3} - \hat{h}_{\text{so},2} \nabla \hat{h}_{\text{so},1} \times \nabla \hat{h}_{\text{so},3} + \hat{h}_{\text{so},3} \nabla \hat{h}_{\text{so},1} \times \nabla \hat{h}_{\text{so},2}] \\ &= \sum_j \frac{1}{8\pi} \epsilon^{mnl} \int_{\text{BIS}_j} d^2\mathbf{k} \cdot \hat{h}_{\text{so},m} (\nabla \hat{h}_{\text{so},n} \times \nabla \hat{h}_{\text{so},l}). \end{aligned} \quad (\text{S13})$$

The last line of the above equation denotes the coverage of the SO field $\hat{\mathbf{h}}_{\text{so}}(\mathbf{k})$ over the 2D spherical surface S^2 when \mathbf{k} runs over the BISs, which implies that the 3D winding number of the bulk is mapped to the 2D Chern number defined on the 2D BISs. As is known that the integral $\frac{1}{8\pi} \epsilon^{mnl} \int_{\text{BIS}_j} d^2\mathbf{k} \cdot \hat{h}_{\text{so},m} (\nabla \hat{h}_{\text{so},n} \times \nabla \hat{h}_{\text{so},l})$ counts the topological charge of the Weyl points at $\mathbf{h}_{\text{so}}(\mathbf{k}) = 0$ of the SO field in the vector area \mathcal{V}_{BIS} enclosed by the BISs.

We also give an example for the 3D topological phases. Consider the B phase of superfluid ^3He [35, 39], which can be treated as a 3D topological superconducting phase in class DIII. The Hamiltonian reads $\mathcal{H}(\mathbf{k}) = h_0(\mathbf{k})\sigma_z \otimes \mathbb{1} + h_1(\mathbf{k})\sigma_x \otimes \sigma_z + h_2(\mathbf{k})\sigma_y \otimes \mathbb{1} + h_3(\mathbf{k})\sigma_x \otimes \sigma_x$ with $\vec{h}(\mathbf{k}) = (\mathbf{k}^2/2m - \mu, k_x, -k_y, -k_z)$. It is easy to see that the system is trivial for $\mu < 0$. For the case with $\mu > 0$, a single Weyl point with $\mathbf{h}_{\text{so}} = (h_1, h_2, h_3) = 0$ at $\mathbf{k} = 0$ and of charge $+1$ is enclosed by the BIS, which renders the system being topologically nontrivial with winding number $\nu_3 = +1$.

4. The generic dD topological phases characterized by integers

As shown in previous cases, the topological phases classified by \mathbb{Z} in 1, 2 and 3 dimensions share a common property that the bulk topology can be characterized by the coverage of the SO field over the spherical surface S^{d-1} when \mathbf{k} runs over the BISs (or the winding of the SO field on the BISs). Actually, it is valid for any dimensions. Generally, the topological phases in $d = 2n - 1$ dimensions are characterized by the $(2n - 1)D$ winding number

$$\nu_{2n-1} = \frac{(-1)^{n-1} (n-1)!}{2(2\pi i)^n (2n-1)!} \int_{\text{BZ}} \text{Tr}[\gamma \mathcal{H} (d\mathcal{H})^{2n-1}] \quad (\text{S14})$$

with

$$\text{Tr}[\gamma \mathcal{H} (d\mathcal{H})^{2n-1}] = (2n-1)! (-2i)^n \sum_{i=0}^{2n-1} \epsilon^{i01\cdots\bar{i}\cdots(2n-1)} h'_i dh'_0 \wedge dh'_1 \wedge \cdots \wedge dh'_i \wedge \cdots \wedge dh'_{2n-1}, \quad (\text{S15})$$

where \bar{i} means that the index does not take the value i , and we have used the trace property of Clifford matrices (see Tab. I) which contributes the factor $(-2i)^n$, while the product of the Levi-Civita tensor and the wedge will lead to the term $(2n-1)! \epsilon^{i01\cdots\bar{i}\cdots(2n-1)} = (2n-1)! (-1)^i$. Similarly, in $d = 2n$ dimensions, the topological phases are characterized by the dD (or the n -th) Chern number

$$\text{Ch}_n = -\frac{1}{2^{2n+1}} \frac{1}{n!} \left(\frac{i}{2\pi}\right)^n \int_{\text{BZ}} \text{Tr}[\mathcal{H} (d\mathcal{H})^{2n}] \quad (\text{S16})$$

with

$$\text{Tr}[\mathcal{H} (d\mathcal{H})^{2n}] = (2n)! (-2i)^n \sum_{i=0}^{2n} \epsilon^{i01\cdots\bar{i}\cdots(2n)} h'_i dh'_0 \wedge dh'_1 \wedge \cdots \wedge dh'_i \wedge \cdots \wedge dh'_{2n}. \quad (\text{S17})$$

From the above, we can obtain that the winding number and Chern number have the same structure and are proportional to the terms $\sum_{i=0}^d (-1)^i h'_i \bar{\bigwedge}_{l=0}^d dh'_l$, where the *wedge product* $\bar{\bigwedge}$ indicates the index $l \neq i$. These terms can be readily calculated with the deformed Hamiltonian (S3): for $i = 0$, we have

$$h'_0 \bar{\bigwedge}_{l=1}^d dh'_l = \sin \Theta_{\mathbf{k}} \cos^d \Theta_{\mathbf{k}} \bar{\bigwedge}_{l=1}^d d\hat{h}_{\text{so},l} + \sin^2 \Theta_{\mathbf{k}} \cos^{d-1} \Theta_{\mathbf{k}} d\Theta_{\mathbf{k}} \wedge \sum_{i=1}^d (-1)^i \hat{h}_{\text{so},i} \bar{\bigwedge}_{l=1}^d d\hat{h}_{\text{so},l}; \quad (\text{S18})$$

and for $i \neq 0$, we obtain

$$h'_i \bar{\bigwedge}_{l=0}^d dh'_l = \cos^{d+1} \Theta_{\mathbf{k}} d\Theta_{\mathbf{k}} \wedge \hat{h}_{\text{so},i} \bar{\bigwedge}_{l=1}^d d\hat{h}_{\text{so},l}. \quad (\text{S19})$$

Therefore,

$$\sum_{i=0}^d (-1)^i h'_i \bar{\bigwedge}_{l=0}^d dh'_l = \sin \Theta_{\mathbf{k}} \cos^d \Theta_{\mathbf{k}} \bar{\bigwedge}_{l=1}^d d\hat{h}_{\text{so},l} + \cos^{d-1} \Theta_{\mathbf{k}} d\Theta_{\mathbf{k}} \wedge \sum_{i=1}^d (-1)^i \hat{h}_{\text{so},i} \bar{\bigwedge}_{l=1}^d d\hat{h}_{\text{so},l}. \quad (\text{S20})$$

Again we take that $\Theta_{\mathbf{k}}$ approaches the step function, and the terms involving $\sin \Theta_{\mathbf{k}} \cos^d \Theta_{\mathbf{k}}$ vanish. The SO field with $\cos \Theta_{\mathbf{k}}$ is non-zero only on the BISs with $\sin \Theta_{\mathbf{k}} = 0$. Hence, the first term in Eq. (S20) can be neglected. One can also decompose the measure $d^d \mathbf{k}$ into $d\mathbf{k}_{\perp} d^{d-1} \mathbf{k}_{\parallel}$, and the integral for the second term can be further reduced to the region \mathcal{R} with non-zero $d\Theta_{\mathbf{k}}$:

$$\begin{aligned} \int_{\text{BZ}} \sum_{i=0}^d (-1)^i h'_i \bar{\bigwedge}_{l=0}^d dh'_l &= \int_{\mathcal{R}} \cos^{d-1} \Theta_{\mathbf{k}} d\Theta_{\mathbf{k}} \wedge \sum_{i=1}^d (-1)^i \hat{h}_{\text{so},i} \bar{\bigwedge}_{l=1}^d d\hat{h}_{\text{so},l} \\ &= \int_{-\pi/2}^{\pi/2} d\Theta_{k_{\perp}} \cos^{d-1} \Theta_{k_{\perp}} \sum_j \int_{\text{BIS}_j} \sum_{i=1}^d (-1)^i \hat{h}_{\text{so},i} \bar{\bigwedge}_{l=1}^d d\hat{h}_{\text{so},l}, \end{aligned} \quad (\text{S21})$$

where we obtain by a straightforward calculation that

$$\int_{-\pi/2}^{\pi/2} dx \cos^{d-1} x = \frac{d-2}{d-1} \int_{-\pi/2}^{\pi/2} dx \cos^{d-3} x = \begin{cases} \frac{(2n-3)!!}{2^{n-1}(n-1)!} \pi & \text{for } d = 2n-1, \\ \frac{2^n (n-1)!}{(2n-1)!!} & \text{for } d = 2n. \end{cases} \quad (\text{S22})$$

Finally, the $(2n-1)$ -dimensional winding number reads

$$\begin{aligned} \nu_{2n-1} &= \sum_j -\frac{(2n-3)!!}{2^n \pi^{n-1}} \int_{\text{BIS}_j} \sum_{i=1}^{2n-1} (-1)^i \hat{h}_{\text{so},i} d\hat{h}_{\text{so},1} \wedge \cdots \wedge d\hat{h}_{\text{so},\bar{i}} \wedge \cdots \wedge d\hat{h}_{\text{so},2n-1} \\ &= \sum_j \frac{(2n-3)!!}{2^n \pi^{n-1}} \frac{1}{(2n-2)!} \int_{\text{BIS}_j} \hat{h}_{\text{so}} (d\hat{h}_{\text{so}})^{2n-2}, \end{aligned} \quad (\text{S23})$$

where the integrand $\hat{h}_{\text{so}}(d\hat{h}_{\text{so}})^{d-1} \equiv \epsilon^{i_1 i_2 \dots i_d} \hat{h}_{\text{so},i_1} d\hat{h}_{\text{so},i_2} \wedge \cdots \wedge d\hat{h}_{\text{so},i_d}$ is defined on the $(d-1)$ D BISs, with the indices $i_1, \dots, i_d \in \{1, \dots, d\}$. Similarly, the n -th Chern number becomes

$$\begin{aligned} \text{Ch}_n &= \sum_j -\frac{(n-1)!}{2\pi^n} \int_{\text{BIS}_j} \sum_{i=1}^{2n} (-1)^i \hat{h}_{\text{so},i} d\hat{h}_{\text{so},1} \wedge \cdots \wedge d\hat{h}_{\text{so},\bar{i}} \wedge \cdots \wedge d\hat{h}_{\text{so},2n} \\ &= \sum_j \frac{(n-1)!}{2\pi^n} \frac{1}{(2n-1)!} \int_{\text{BIS}_j} \hat{h}_{\text{so}} (d\hat{h}_{\text{so}})^{2n-1}. \end{aligned} \quad (\text{S24})$$

In summary, both the winding number and Chern number can be expressed in a unified form as the winding of the SO field \hat{h}_{so} along the BISs:

$$w_{d-1} = \sum_j \frac{\Gamma(d/2)}{2\pi^{d/2}} \frac{1}{(d-1)!} \int_{\text{BIS}_j} \hat{h}_{\text{so}} (d\hat{h}_{\text{so}})^{d-1}, \quad (\text{S25})$$

where $\Gamma(x)$ is the Gamma function with $\Gamma(x+1) = x\Gamma(x)$, $\Gamma(1) = 1$ and $\Gamma(1/2) = \sqrt{\pi}$. Note that the prefactor $2\pi^{d/2}/\Gamma(d/2)$ is actually the area of a unit sphere in d dimensions. Analogous to the ‘‘Gauss’s law’’ in the previous 2D and 3D cases, the invariant w_{d-1} simply counts the total topological charges, e.g., Dirac points in 2D and Weyl points in 3D cases, of the SO field enclosed by the BISs:

$$w_{d-1} = \sum_{i \in \mathcal{V}_{\text{BIS}}} \mathcal{C}_i, \quad (\text{S26})$$

where

$$\mathcal{C}_i \equiv \frac{\Gamma(d/2)}{2\pi^{d/2}} \frac{1}{(d-1)!} \int_{\text{BIS}_i} \hat{h}_{\text{so}} (d\hat{h}_{\text{so}})^{d-1} \quad (\text{S27})$$

represents the total topological charge in the patch of \mathcal{V}_{BIS} enclosed by the i -th BIS. The topological phase transition happens when a charge is added to or removed from the region enclosed by the BISs, as the gap must be closed and reopen when the topological charge with $\mathbf{h}_{\text{so}} = 0$ passes through the BISs which correspond to $h_0 = 0$. Accordingly, the topology characterized by the SO field on BISs is changed. With these results we have predicted a remarkable bulk-surface duality that the characterization of the topology for a d D topological phase can generically be mapped to the topological invariant defined on the $(d-1)$ D BISs.

5. Generalization to generic multiband systems

We show here that the results in Eqs. (S25) and (S26) based on the d D minimal topological Hamiltonian (S1) are valid for the generic systems with arbitrary multiple bands and multiple band crossings in the BZ, as illustrated Fig. S2c. Note that for a generic d D topological phase, the gap must be opened through each group of n_d bands ($n_d = 2^{d/2}$ or $2^{(d+1)/2}$) with hybridization at BISs of these bands. For convenience, we denote each band crossing for a group of n_d bands as a BIS. Without changing the topology of the system, we assume that each BIS is separated from others in the BZ (If there are more than one BIS occurring at the same \mathbf{k} point, one can continuously deform the

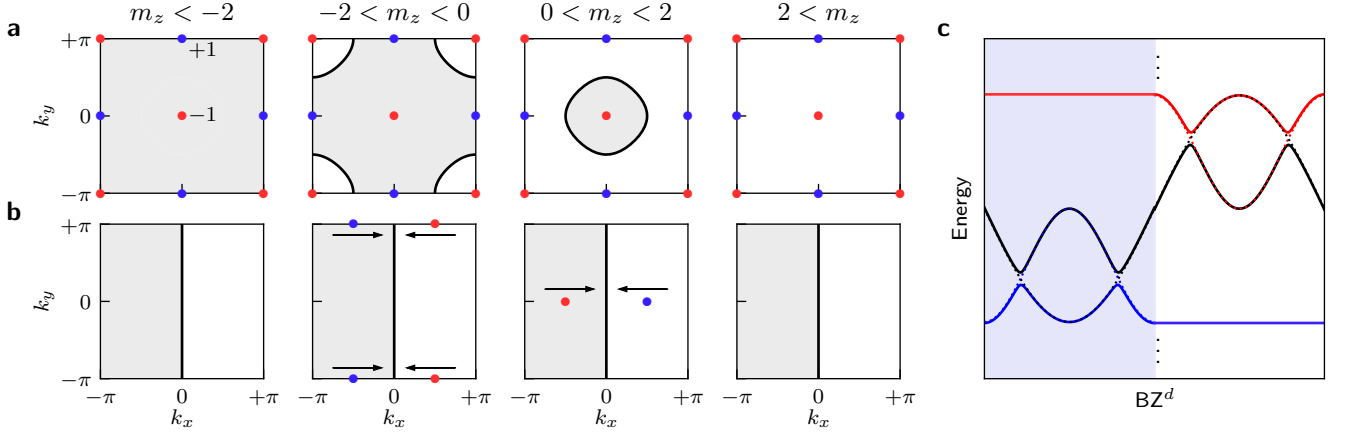


Figure S2: **Charge configurations of the 2D model and schematic diagram of the multi-band case.** **a-b**, The configurations of topological charges by taking that $h_0 = m_z - t_0 \cos k_x - t_0 \cos k_y$ (**a**) and $h_0 = t_{so} \sin k_x$ (**b**), respectively. Here the red (blue) circle denotes the charge -1 ($+1$), and the gray region represents $h_0(\mathbf{k}) < 0$ (i.e., \mathcal{V}_{BIS}) with black line being the BIS. **c**, A schematic diagram for multiple bands with (solid lines) or without (dotted lines) the SO field. Here different background colors indicate different patches.

band dispersion and separate such BISs without affecting the bulk topology). In this case, the Hamiltonian around each BIS can be decomposed to the contributions from three parts: the n_d bands with hybridization on the BIS, the bands with energy above the BIS, and the bands below the BIS. Thus the Hamiltonian can be locally written as $\mathcal{H}(\mathbf{k}) = \mathcal{P}_{\text{upper}}(\mathbf{k}) \oplus \mathcal{H}_{\text{BIS}}(\mathbf{k}) \oplus \mathcal{P}_{\text{lower}}(\mathbf{k})$. Here $\mathcal{P}_{\text{upper/lower}}$ are the projection operators for the bands with higher (lower) energy than the part with band crossing \mathcal{H}_{BIS} . For the higher or lower bands $\mathcal{P}_{\text{upper/lower}}$, as there is no band crossing, the corresponding spin textures are trivial and no singularities exist for the corresponding eigenstates. We can safely deform the bands of $\mathcal{P}_{\text{upper/lower}}$ into constants in dispersion. Similarly, away from the BISs, no band crossing occurs, so all the bands can be smoothly connected in those areas of the BZ, and also be further deformed into constants in dispersion. It is straightforward to know that the flattened paths in BZ have no contribution to the bulk topology, which is then solely determined from the integral over the BISs. Further, to compute the contribution from a specific BIS, we can single out the n_d bands which are characterized by the Hamiltonian $\mathcal{H}_{\text{BIS}}(\mathbf{k})$ on the BIS, and flatten these bands in all the remaining \mathbf{k} space of BZ away from such BIS. This can be safely done since the band crossings occurring at other momenta of BZ are unrelated to the contribution to bulk topology from the BIS under consideration (thus those band crossings can be removed for this computation). In this way, the contribution of the BIS is effectively determined by a basic Hamiltonian with the band crossing at BIS described by $\mathcal{H}_{\text{BIS}}(\mathbf{k})$, precisely given by the $(d-1)$ D topological number defined on the BIS. The total topological invariant of the d D phase is then a summation of contributions from all BISs, formed by all bands of the BZ. This completes the proof.

With the above proof we conclude that the $(d-1)$ D topological number shown in Eq. (S25) can classify the generic d D phases with multiple bands and multiple crossings, while the summation in the equation of w_{d-1} runs over all BISs formed by all the relevant bands of the d D topological phase. Nevertheless, we should emphasize that, in the generic case, the SO field $\mathbf{h}_{\text{so}}(\mathbf{k})$ should be defined locally on the corresponding BIS, characterizing only the hybridization among the n_d bands of such BIS.

II. Dynamical Classification of Topological Phases

Now we develop the dynamical classification of the topological phases based on the bulk-surface duality shown above. We need to address two basic issues. The first is that we shall work out the characterization of the BISs by quantum dynamics. The second is that we further establish the classification of the topological phase by quantum dynamics on the BISs. The study is based on the basic Hamiltonian (S1), while the results can be directly applied to generic multiband systems.

A. Characterizing the BISs by quench dynamics

We consider the quench process realized by tuning $h_0(\mathbf{k}) = m_0 + \tilde{h}_0(\mathbf{k})$ from a deep trivial regime with $m_0|_{t<0} \gg \max[|\tilde{h}_0(\mathbf{k})|]$ to a topological regime $m_0|_{t>0} \lesssim \max[|\tilde{h}_0(\mathbf{k})|]$. Here $\tilde{h}_0(\mathbf{k})$ represents momentum-dependent field and m_0 demotes a constant ‘magnetization’. Initially, the system is prepared in the ground state of the pre-quench Hamiltonian $\mathcal{H}(m_0|_{t<0}, \mathbf{k})$ in the deep trivial regime, with density matrix ρ_0 , where the spins are fully polarized in the opposite direction of the axes h_0 . After a sudden quench to a topological non-trivial Hamiltonian $\mathcal{H}(m_0|_{t>0}, \mathbf{k})$, each momentum-linked spin will rotate around the post-quench vector field $\vec{h}(\mathbf{k})$, with the quantum dynamics being governed by the unitary evolution operator $U(t) = \exp(-i\mathcal{H}t)$ for the post-quench system, see Fig. S3.

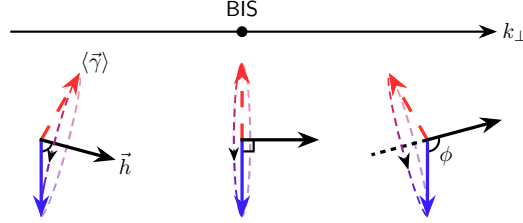


Figure S3: **Schematic diagram of quench dynamics.** The initial state (blue arrows) is prepared in the ground state of the pre-quench Hamiltonian and is highly polarized by $h_0(\mathbf{k})$. After a sudden quench to a topological phase, each momentum-linked spin will precess around the post-quench vector field $\vec{h}(\mathbf{k})$ (black arrows). Here ϕ denotes the angle between the pre-quench spins and the post-quench vector field $\vec{h}(\mathbf{k})$.

We consider the time-averaged spin polarizations, which can be measured in experiments:

$$\overline{\langle \gamma_i \rangle} = \lim_{T \rightarrow \infty} \frac{1}{T} \int_0^T dt \text{Tr} [\rho_0 e^{i\mathcal{H}t} \gamma_i e^{-i\mathcal{H}t}]. \quad (\text{S28})$$

For the Hamiltonian (S1), one can show that $e^{i\mathcal{H}t} = \cos(Et) + i \sin(Et)\mathcal{H}/E$ with $E(\mathbf{k}) = \sqrt{\sum_{i=0}^d h_i^2}$ the energy. Therefore, the time-averaged spin polarizations become

$$\overline{\langle \gamma_i(\mathbf{k}) \rangle} = \frac{h_i \text{Tr} [\rho_0 \mathcal{H}]}{E^2}. \quad (\text{S29})$$

On the BISs defined by $h_0(\mathbf{k}) = 0$ for the post-quench Hamiltonian, one can find that $\overline{\langle \gamma_0 \rangle}$ vanishes. Moreover, since the pre-quench spins polarized in the axes h_0 are perpendicular to the SO field $\mathbf{h}_{\text{so}}(\mathbf{k})$, we can obtain that $\text{Tr} [\rho_0 \mathcal{H}]$ is governed by h_0 , which is however zero on BIS by definition, and therefore vanishes on the BISs. As a result, all the time-averaged spin polarizations $\overline{\langle \gamma_i(\mathbf{k}) \rangle}$ (for $i = 0, 1, \dots, d$) vanish on the BISs. This can be intuitively understood by the spin precession within the plane perpendicular to the post-vector field $\vec{h}(\mathbf{k}) = \mathbf{h}_{\text{so}}(\mathbf{k})$ on the BISs, see Fig. S3. Hence, the BISs can be dynamically determined by the surface with vanishing time-averaged spin polarizations:

$$\text{BIS} = \{\mathbf{k} | \overline{\langle \vec{\gamma}(\mathbf{k}) \rangle} = 0\}. \quad (\text{S30})$$

B. Dynamical topological invariants and the dynamical bulk-surface duality

Since all time-averaged spin polarizations $\overline{\langle \gamma_i \rangle}$ vanish on the BISs, we cannot read out the information of the corresponding SO field directly from $\overline{\langle \gamma_i \rangle}$. We notice that the vector field $\vec{h}(\mathbf{k})$ deviates from the SO field $\mathbf{h}_{\text{so}}(\mathbf{k})$ due to the non-zero h_0 near the BISs, which results in non-zero spin projection along the SO field. On the other hand, the opposite signs of $h_0(\mathbf{k})$ in the two sides of BISs lead to a dramatic variation of the time-averaged spin textures across the BISs, e.g., see Fig. S3. When passing through the BISs, the relative angle ϕ between the pre-quench spin and the post-quench vector field $\vec{h}(\mathbf{k})$ varies from $\phi < \pi/2$ in the \mathcal{V}_{BIS} with the time-averaged polarization $\overline{\langle \vec{\gamma} \rangle}$ being along the direction of the vector $\vec{h}(\mathbf{k})$, to $\phi > \pi/2$ in the region $\bar{\mathcal{V}}_{\text{BIS}}$ with the time-averaged polarization along negative direction of $\vec{h}(\mathbf{k})$. As to be proven in the following, the variation of time-averaged polarization $\overline{\langle \vec{\gamma} \rangle}$ across BISs is related to the SO field $\mathbf{h}_{\text{so}}(\mathbf{k})$, and can be applied to characterize the topology.

As before, the momentum \mathbf{k} can be decomposed into $(k_\perp, \mathbf{k}_\parallel)$ with k_\perp perpendicular to the contour of $h_0(\mathbf{k}) = 0$ and pointing to the region $\bar{\mathcal{V}}_{\text{BIS}}$ with $h_0(\mathbf{k}) > 0$. Here we focus on the regime with $h_0(\mathbf{k}) \gg 0$ in the entire BZ for the pre-quench Hamiltonian, i.e., the initial spin is highly polarized in the opposite direction of γ_0 . To characterize the topology, a new dynamical spin-texture field can be defined as the directional derivative of time-averaged spin textures $\overline{\langle \vec{\gamma} \rangle}$ across the BISs:

$$\widetilde{\mathbf{g}}(\mathbf{k}) \equiv -\frac{1}{\mathcal{N}_{\mathbf{k}}} \partial_{k_\perp} \overline{\langle \vec{\gamma} \rangle} = -\lim_{k_\perp \rightarrow 0^+} \frac{1}{\mathcal{N}_{\mathbf{k}}} \frac{\Delta \overline{\langle \vec{\gamma} \rangle}}{2k_\perp} = -\lim_{k_\perp \rightarrow 0^+} \frac{1}{\mathcal{N}_{\mathbf{k}}} \frac{\overline{\langle \vec{\gamma} \rangle}|_{h_0(k_\perp) > 0} - \overline{\langle \vec{\gamma} \rangle}|_{h_0(-k_\perp) < 0}}{2k_\perp}, \quad (\text{S31})$$

where $\mathcal{N}_{\mathbf{k}}$ is the normalization factor of the new field $\widetilde{\mathbf{g}}(\mathbf{k})$, and the origin of k_\perp has been shifted locally to the BISs. If the initial state ρ_0 is polarized in the opposite direction of the axes h_0 , the time averaged spin polarizations become

$$\overline{\langle \gamma_i(\mathbf{k}) \rangle} = -h_i(\mathbf{k})h_0(\mathbf{k})/E^2(\mathbf{k}). \quad (\text{S32})$$

It is worthwhile to note that for the pre-quench Hamiltonian with $h_0(\mathbf{k}) \ll 0$, the time averaged spin polarizations $\overline{\langle \gamma_i \rangle} = +h_i h_0/E^2$. Accordingly, the dynamical spin-texture field should be defined by $\widetilde{\mathbf{g}}(\mathbf{k}) = \partial_{k_\perp} \overline{\langle \vec{\gamma} \rangle}$, which takes an additional minus sign. Near the BISs, the dispersion $h_0(\mathbf{k})$ is monotonous and is determined by k_\perp uniquely. We can identify h_0 from k_\perp , that is, $h_0 \cong k_\perp$ up to some local scale transformation that does not affect the topology. The difference of $\overline{\langle \gamma_i \rangle}$ between the two sides of BISs reads

$$\Delta \overline{\langle \gamma_i \rangle} \cong -\left[\frac{h_i(k_\perp, \mathbf{k}_\parallel)k_\perp}{k_\perp^2 + \sum_{j=1}^d h_j^2(k_\perp, \mathbf{k}_\parallel)} - \frac{h_i(-k_\perp, \mathbf{k}_\parallel)(-k_\perp)}{k_\perp^2 + \sum_{j=1}^d h_j^2(-k_\perp, \mathbf{k}_\parallel)} \right] = -2 \frac{h_i(0, \mathbf{k}_\parallel)k_\perp}{\sum_{j=1}^d h_j^2(0, \mathbf{k}_\parallel)} + \mathcal{O}(k_\perp^2). \quad (\text{S33})$$

We further obtain the emergent dynamical spin-texture field by

$$\widetilde{g}_i(\mathbf{k}) = \frac{h_i(0, \mathbf{k}_\parallel)}{\sum_{j=1}^d h_j^2(0, \mathbf{k}_\parallel)} = \hat{h}_{\text{so},i}. \quad (\text{S34})$$

This is a novel result showing that the SO field $\mathbf{h}_{\text{so}}(\mathbf{k})$ maps to an emergent dynamical field. With this result we obtain immediately that the bulk topology can be characterized by a dynamical invariant defined as the winding of the new dynamical spin-texture field $\widetilde{\mathbf{g}}(\mathbf{k})$ on the BISs:

$$w_{d-1} \equiv \sum_j \frac{\Gamma(d/2)}{2\pi^{d/2}} \frac{1}{(d-1)!} \int_{\text{BIS}_j} \widetilde{\mathbf{g}}(\mathbf{k}) [d\widetilde{\mathbf{g}}(\mathbf{k})]^{d-1}. \quad (\text{S35})$$

This renders the dynamical classification of the generic dD topological phase with integer topological invariants.

The right hand side of the formula (S35) describes the mapping from the BISs to $(d-1)D$ spherical surface of which the emergent dynamical field $\widetilde{\mathbf{g}}(\mathbf{k})$ are elements. Intuitively, the dynamical topological invariant is described by the coverage of the emergent dynamical spin-texture $\widetilde{\mathbf{g}}(\mathbf{k})$ over the full $(d-1)D$ spherical surface. For example, in the 1D topological phase, the dynamical field $\widetilde{\mathbf{g}}(\mathbf{k})$ should point to opposite directions in the two band inversion points. For the 2D phase, the nontrivial topology necessitates that the field $\widetilde{\mathbf{g}}(\mathbf{k})$ exhibits 1D winding along the band inversion rings. Further, for the 3D topological phase, the field $\widetilde{\mathbf{g}}(\mathbf{k})$ should exhibit 2D topological skyrmion structure on the BISs. These results manifest a novel dynamical *bulk-surface* correspondence.

The dynamical classification provides fundamentally new strategies of experimental feasibility to measure topological phases. First, the bulk-surface duality enables a much simplified scheme to characterize the dD topological phases by lower-dimensional topological numbers. Secondly, while the BISs for the equilibrium phases may not be easy to identify, even they are well defined with $\mathbf{h}_0(\mathbf{k}) = 0$, since the configuration of BISs for a generic system could be complicated, all the information of the BISs automatically show up in the quench dynamics. In particular, in the dynamical regime the BISs are characterized by the \mathbf{k} points with vanishing time-averaged spin-polarizations, which can be directly measured in experiment. Finally, the bulk topology of the dD phase can be further determined from the dynamical spin-polarization patterns emerging on the BISs. The measurements based on dynamical classification of the topological phases can lead to a fundamentally new approach to detect the topological quantum phases with high feasibility.

III. Numerical Results

In this section, we shall provide more details of numerical results, which serve as a supplement to the main text and complete the demonstration of experimental feasibility of the detecting strategy based on dynamical classification.

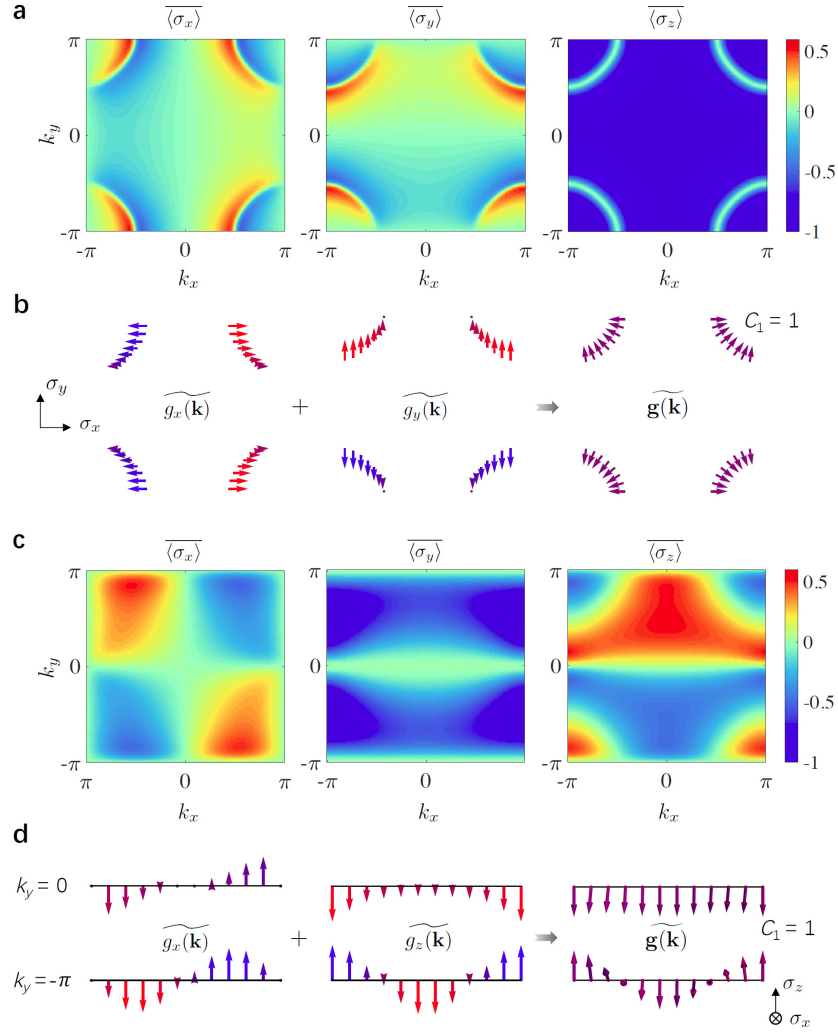


Figure S4: **Quenching to the topological phase with $C_1 = 1$.** **a-b**, Quenching the h_z axis. Time-averaged spin textures are measured after a sudden quench from $m_z = 8t_0$ to $-t_0$ (**a**), with BISs being characterized by $\langle \vec{\sigma} \rangle = 0$ (the green ring centered at (π, π)). The $\mathbf{g}(\mathbf{k})$ field is obtained by combining the derivatives $\partial_{k_\perp} \langle \sigma_{x,y} \rangle$ (**b**), and gives the Chern number $C_1 = 1$. Here $t_{\text{so}}^{x,y}$ both take $0.2t_0$. **c-d**, Quenching the h_y axis. Time-averaged spin textures (**c**) and the dynamical field $\mathbf{g}(\mathbf{k})$ on BISs (**d**) are shown after a quench from $m_y = 50t_0$ to 0 with $m_z = -t_0$. The BISs determined by $\langle \vec{\sigma} \rangle = 0$ are identified to $k_y = 0, -\pi$, and the non-zero winding number of the dynamical spin-texture field along $k_y = -\pi$ characterizes the Chern number $C_1 = 1$. Here we set $t_{\text{so}}^x = t_0$ and $t_{\text{so}}^y = 2t_0$.

A. Characterizing quantum anomalous Hall insulators

The 2D quantum anomalous Hall (QAH) model generally reads $\mathcal{H}(\mathbf{k}) = \vec{h}(\mathbf{k}) \cdot \vec{\sigma}$ with $\vec{h}(\mathbf{k}) = (m_x + t_{\text{so}}^x \sin k_x, m_y + t_{\text{so}}^y \sin k_y, m_z - t_0 \cos k_x - t_0 \cos k_y)$, which has been realized in Ref. [28, 29]. Here we identify the topological phases by m_z ($m_x = m_y = 0$): (i) $0 < m_z < 2t_0$ with the Chern number $C_1 = -1$; (ii) $-2t_0 < m_z < 0$ with $C_1 = 1$; (iii) being trivial for $|m_z| > 2t_0$. The flexibility in the decomposition of the vector $\vec{h}(\mathbf{k})$ allows us to consider different quench ways to detect the topology. As discussed in the main text, we can take $h_0 \equiv h_z$, $\mathbf{h}_{\text{so}} \equiv (h_x, h_y)$, and the quench is performed by varying m_z , which corresponds to quenching the h_z axis. Alternatively, we can also take $h_0 \equiv h_y$ and quench the h_y axis by ramping m_y quickly from $|m_y| \gg t_0$ to 0 while fixing m_z . These two quench ways leads to distinct observations, but can be both used to distinguish different topological phases. The only thing to be noted is that the ratios $t_{\text{so}}^{x,y}/t_0$ should be properly adjusted to clarify the observation in the two quench ways.

When quenching the h_z axis, we set $t_{\text{so}}^x = t_{\text{so}}^y = 0.2t_0$, and suddenly change m_z from the deep trivial phase $|m_z| \gg 2t_0$ to one of the two topological phases. In Fig. 2a-b of the main text, we have shown the results of quenching

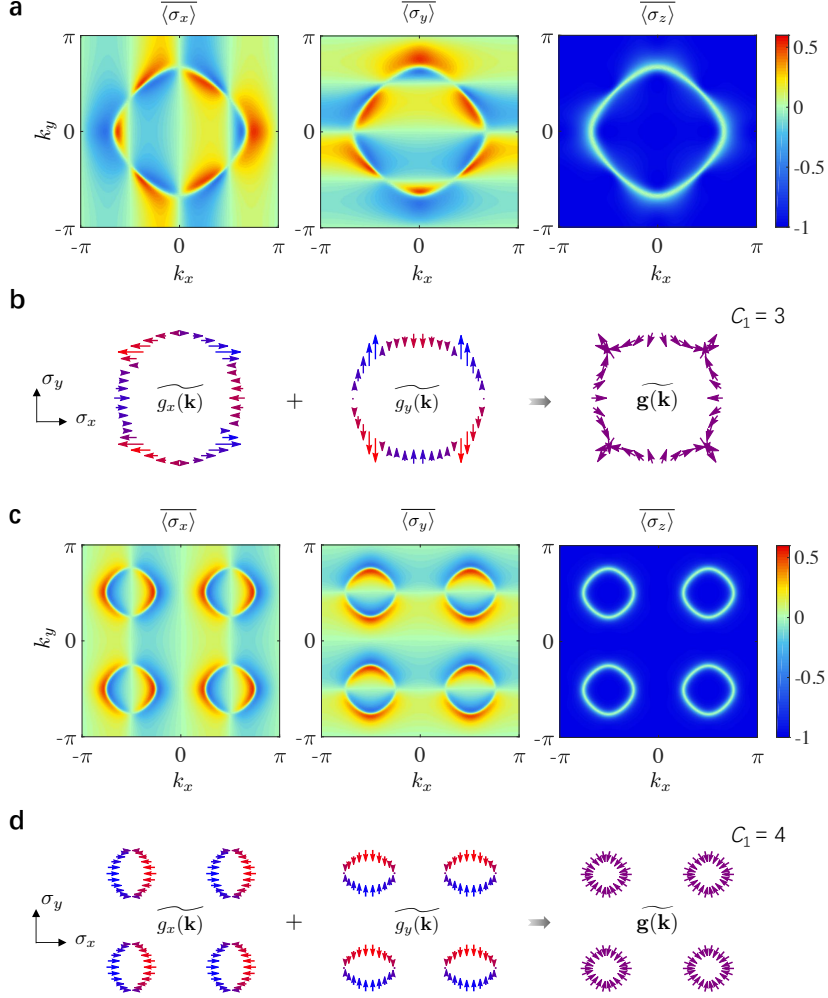


Figure S5: **2D topological phases with high Chern numbers.** **a-b**, Dynamical results of the model \mathcal{H}_1 in section III(B). Time-averaged spin textures **(a)** also exhibit a ring structure for the BIS. But the emergent dynamical field **(b)** winds three circles, corresponding to $C_1 = 3$. The results are obtained by a quench from $m_z = 8t_0$ to $0.5t_0$ with $t_{so} = 0.2t_0$. **c-d**, Dynamical results of the model \mathcal{H}_2 of section III(B). Time-averaged spin textures **(c)** show four rings, and each contributes a full winding **(d)**, charactering the Chern number $C_1 = 4$. The quench is taken from $m_z = 8t_0$ to $-t_0$ with $t_{so} = 0.2t_0$.

to the phase (i). Here we provide the results of the phase (ii) in Fig. S4a-b. As discussed in the former sections, the vanishing time-averaged spin texture $\langle \vec{\sigma} \rangle = 0$ characterizes the BISs, and the dynamical spin-texture field, defined as $\widetilde{\mathbf{g}}(\mathbf{k}) = -\partial_{k_\perp} \langle \vec{\sigma} \rangle$ across the BISs, signifies the SO field $\hat{\mathbf{h}}_{so}(\mathbf{k})$ and can be used to classify the topology. Compared to Fig. 2a-b in the main text, the BIS in Fig. S4a becomes a ring centered at $\mathbf{k} = (\pi, \pi)$ rather than at $(0, 0)$. Here the region enclosed by the BIS, i.e. \mathcal{V}_{BIS} , contains three topological charges of the SO field: one charge -1 located at $(0, 0)$ and other two charges $+1$ at $(0, \pi)$ and $(\pi, 0)$, which indicates the Chern number $C_1 = 1$ and can be reflected by the winding of the spin-texture field $\widetilde{\mathbf{g}}(\mathbf{k})$ along the BIS.

When quenching the h_y axis, we set $t_{so}^x = t_0$ and $t_{so}^y = 2t_0$. In this quench way, the BISs are the same for different topological regimes, and are identified to two lines $k_y = -\pi$ and $k_y = 0$. However the dynamical spin-texture field on the BISs should be different, which classifies the different topology, as shown in Fig. 2c-d for $C_1 = -1$ and in Fig. S4c-d for $C_1 = 1$. In Fig. 2c-d, the emergent dynamical spin-texture field $\widetilde{\mathbf{g}}(\mathbf{k})$ winds clockwise along $k_y = 0$ in the σ_x - σ_z plane while the winding along $k_y = -\pi$ is zero. The situation becomes reverse in Fig. S4c-d, where the spin-texture field $\widetilde{\mathbf{g}}(\mathbf{k})$ winds anti-clockwise along $k_y = -\pi$ and becomes trivial along $k_y = 0$, which characterizes the Chern number $C_1 = 1$.

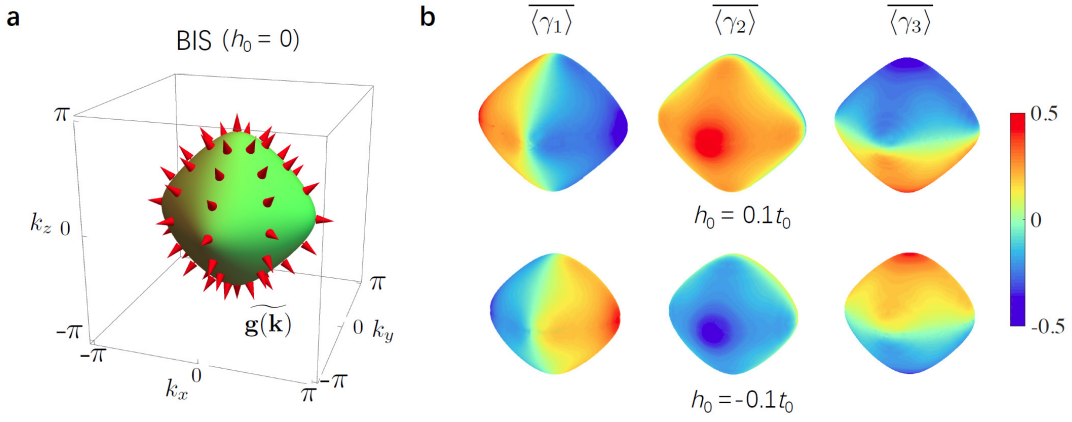


Figure S6: **Numerical results of the 3D model.** The BIS of the topological phase with 3D winding number $\nu_3 = -1$ is a 2D closed surface (a). The dynamical field $\vec{g}(\mathbf{k}) = -\partial_{k_\perp} \overline{\langle \vec{\gamma} \rangle}$ can be read out from the time-averaged spin textures $\overline{\langle \gamma_j \rangle}$ ($j = 1, 2, 3$) on two equal-energy surfaces $h_0 = \pm 0.1t_0$ (b). The results are obtained by spin dynamics of two orbits after a quench from $m_z = 8t_0$ to $1.3t_0$, with $t_{so} = 0.2t_0$.

B. Topological phases with high invariant

The present detecting strategy based on dynamical classification is certainly applicable to topological phases with high invariants. To illustrate the validity, we consider two different 2D models $\mathcal{H}_j(\mathbf{k}) = \vec{h}_j(\mathbf{k}) \cdot \vec{\sigma}$ ($j = 1, 2$), which are variations of the 2D QAH model studied in the above section.

We consider the first model \mathcal{H}_1 with the vector field $\vec{h}_1(\mathbf{k}) = (t_{so} \sin 2k_x, t_{so} \sin 2k_y, m_z - t_0 \cos k_x - t_0 \cos k_y)$. While the trivial phase corresponds to $|m_z| > 2t_0$, the topological phases are distinguished as: (i) $t_0 < m_z < 2t_0$ with the Chern number $C_1 = -1$; (ii) $0 < m_z < t_0$ with $C_1 = 3$; (iii) $-t_0 < m_z < 0$ with $C_1 = -3$; (iv) $-2t_0 < m_z < -t_0$ with $C_1 = 1$. When $t_0 \gg t_{so}$, this model has almost the same band structure as the 2D model in the above section. It is then supposed that the results of quenching to the phases with $C_1 = \pm 1$ should be similar to those shown in Fig. 2a and in Fig. S4a. Here we only provide the numerical results of quenching to the phase with $C_1 = 3$ (see Fig. S5a-b), where the time-averaged spin textures also exhibit ring-shape structure, but the corresponding spin-texture field winds around three times, characterizing the high Chern number.

We then consider the other one \mathcal{H}_2 with $\vec{h}_2(\mathbf{k}) = (t_{so} \sin 2k_x, t_{so} \sin 2k_y, m_z - t_0 \cos 2k_x - t_0 \cos 2k_y)$. Apart from the trivial phase with $|m_z| > 2t_0$, this model has two topological phases: (i) $0 < m_z < 2t_0$ with the Chern number $C_1 = -4$; (ii) $-2t_0 < m_z < 0$ with $C_1 = 4$. After a sudden quench from $m_z \gg 2t_0$ to $|m_z| < 2t_0$, the time-averaged spin textures have four rings (see Fig. S5c-d), and the dynamical spin-texture field on each ring winds around once. Thus four rings in the BZ characterize the Chern number $C_1 = \pm 4$.

C. Characterizing 3D topological phases

Similar to the 1D or 2D topological phases, one can also detect the BISs and the topology of 3D systems by utilizing time-averaged spin textures. As discussed in the main text, the 3D model $\mathcal{H} = \vec{h}(\mathbf{k}) \cdot \vec{\gamma}$, which is a direct generalization of the 2D model (see the main text), has three topological phases. In Fig. 3 of main text, we show the BIS of the topological phase with 3D winding number $\nu_3 = -1$ and the time-averaged spin texture $\overline{\langle \gamma_3 \rangle}$. Here we provide more results and further show that the emergent dynamical spin-texture field $\vec{g}(\mathbf{k})$ on the BIS can be directly read out from the difference of $\overline{\langle \gamma_j \rangle}$ ($j = 1, 2, 3$) on the two equal-energy surfaces slightly outside ($h_0 = 0.1t_0$) and inside ($h_0 = -0.1t_0$) the BIS (see Fig. S6).

D. Detecting topology via dissipative dynamics

The dynamical classification can be generalized to the dissipative quantum dynamics at finite temperature. The spin dynamics can be described by the so-called Lindblad master equation [43, 44]. As shown in the main text, after

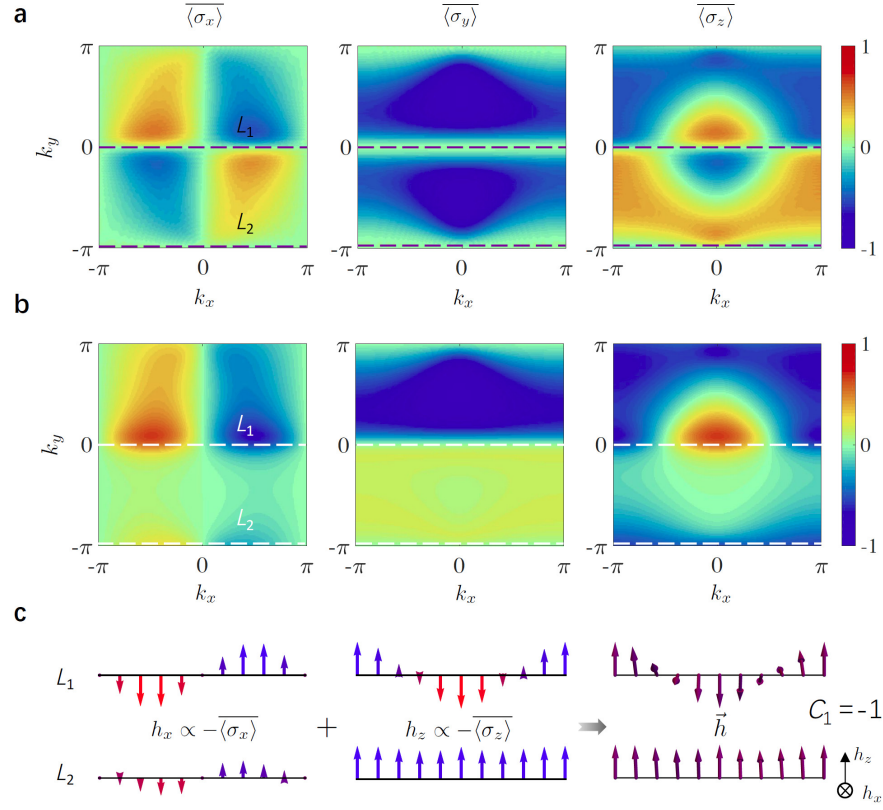


Figure S7: **Classifying topology via dissipative dynamics after quench in h_y axis.** **a**, Spin textures of the 2D model averaged over a short period of $25/t_0$, which can be used to identify the BIS by $\langle \vec{\sigma} \rangle = 0$. Here the two lines $L_{1,2}$ (dashed) are approximate to the BISs. **b**, Time-averaged spin textures over a long period of $600/t_0$, which directly indicate the SO field on the BISs (see **c**). **c**, The direction of the SO field is reflected by $h_{x,z} \propto -\langle \sigma_{x,z} \rangle$. Thus the winding of the SO field along the BISs can be read out from the spin polarizations (in **b**) on the two lines $L_{1,2}$. The non-zero winding along L_1 characterizes the Chern number $C_1 = -1$. Here the dissipative rate is $\eta = 0.003$. Other quench parameters are taken the same as in Fig. 2c of the main text.

a such quench, the dissipation drives the occupation of Bloch states to approach the equilibrium result, and the spin polarization $\langle \vec{\gamma} \rangle$ approaches to be polarized in the reverse direction of the vector $\vec{h}(\mathbf{k})$ after a long-time evolution. Therefore, the dissipation can be exploited as an alternative tool to detect the topology.

In Fig. 4 of the main text, we take the 2D model as an example, and illustrate the detecting method by quenching the h_z axis. Here we consider another case of quenching the h_y axis (in contrast to the results shown in Fig. 2c-d). In Fig. S7a, we present short-time-averaged spin textures, where two lines $L_{1,2}$ that satisfy $\langle \vec{\sigma} \rangle = 0$ can be treated as the BISs approximately. After taking long-time averages (Fig. S7b), we obtain non-zero spin polarizations $\langle \sigma_{x,z} \rangle$ on the BISs, which directly reveal the direction of the vector field $\vec{h}(\mathbf{k}) = \mathbf{h}_{\text{so}}(\mathbf{k})$ by $h_{x,z} \propto -\langle \sigma_{x,z} \rangle$. The winding of the SO field on the BISs is readily obtained via the spin polarizations on the two lines $L_{1,2}$ (Fig. S7c), and the non-zero winding on L_1 or L_2 then characterize the topological number of the post-quench phase.